

Alkali recondensation into chondrules

Emmanuel Jacquet^a, Yves Marrocchi^b, Sébastien Charnoz^c

^a*Institut de Minéralogie, de Physique des Matériaux et de Cosmochimie, Muséum national d'Histoire naturelle, CNRS, CP52, 57 rue Cuvier, Paris, 75005, France*

^b*Centre de Recherches Pétrographiques et*

Géochimiques, , Vandoeuvre-lès-Nancy, 54501, France

^c*Institut de Physique du Globe de Paris, Université de Paris, CNRS, 1 rue Jussieu, Paris, 75005, France*

Abstract

While sub-mm melt droplets should rapidly lose alkali elements in a vacuum at liquidus temperatures, chondrules are only modestly depleted in them (by less than one order of magnitude). The detection of sodium in olivine cores has previously suggested very high saturating partial pressures of gaseous sodium, but we show that alkalis were lost during heating and recondensed at lower temperatures, essentially in the present-day chondrule mesostases. This recondensation was accompanied by mass-dependent enrichment in light isotopes (for multi-isotope alkalis such as K and Rb), but its limited extent indicates a cooling acceleration (or "quenching"). The isotopic fractionation also constrains the ratio of the chondrule density and the cooling rate prior to the quench around 10^{-6} kg.m⁻³.K⁻¹.h suggesting densities above $\sim 10^{-6}$ kg/m³. In a nebular context, this is achievable by radial and vertical concentrations near pressure bumps.

Keywords:

Meteorites, Solar Nebula, Cosmochemistry

1. Introduction

Chondrules are sub-millimeter spheroidal droplets ubiquitous in primitive meteorites (or chondrites). It is largely accepted that chondrules result from magmatic processes involving maximum temperatures in the range 1600–2000 K (Jones et al., 2018), but their formation conditions and the physical process(es) operating are still hotly debated (see Marrocchi et al. (2024) for a review). Mounting evidence of calcium-aluminum-rich inclusions (CAI) or

amoeboid olivine aggregates (AOA) among their precursors, either in the form of identifiable relicts (e.g. Krot et al., 2006; Marrocchi et al., 2018, 2019; Piralla et al., 2021) or bulk chemical (e.g. Misawa and Nakamura, 1988; Jacquet and Marrocchi, 2017) or isotopic (Gerber et al., 2017; Schneider et al., 2020) signatures, suggests "nebular scenarios" where pristine nebular solid aggregates were melted, e.g. by shock waves (Desch et al., 2005; Boley et al., 2013), lightning discharges (Desch and Cuzzi, 2000; Johansen and Okuzumi, 2018), or intermittently exposed magma oceans (Herbst and Greenwood, 2019).

Yet, chondrules also carry signatures of high solid densities in their formation regions, which have given some support to "planetary scenarios" involving impacts (Asphaug et al., 2011; Sanders and Scott, 2012). The frequency of compound chondrules (Gooding and Keil, 1981; Sekiya and Nakamura, 1996; Jacquet, 2021), the Fa contents of chondrule olivine (Grossman et al., 2012; Tenner et al., 2015), and the limited Mg isotopic fractionation of bulk chondrules (Cuzzi and Alexander, 2006) indicate dust densities above $\sim 10^{-6}\text{kg/m}^3$ with a dust/gas ratio enhanced by 1-3 orders of magnitude above solar (Jacquet et al., 2024). Conceivably though, a combination of radial concentration, e.g. around pressure maxima, commonly invoked to explain rings in present-day protoplanetary disks, and settling in a nonturbulent nebula could bring dust concentrations to such levels near the disk midplane, hovering around the threshold for streaming instability and planetesimal accretion (Jacquet et al., 2024).

However, a further constraint threatens to make this hard-fought solution hopelessly inadequate: the abundance of alkali elements, in particular sodium (the most abundant one). Indeed, these moderately volatile elements would be expected to be rapidly lost (within a minute) in vacuum upon heating (Tsuchiyama et al., 1981; Yu et al., 2003; Fedkin and Grossman, 2013). They certainly are depleted in type I chondrules (that is, reduced chondrules, with silicate $\text{Fe}\#\equiv\text{Fe}/(\text{Fe} + \text{Mg}) < 10\text{ mol\%}$), but by less than one order of magnitude, and type II (oxidized) chondrules show almost chondritic levels (Hewins, 1991). While very brief heating (with unimpeded radiative cooling) could avert sodium loss (Hewins, 1991; Rubin and Wasson, 2005; Baecker et al., 2017), estimated cooling times are generally longer by a few orders of magnitude (Jones et al., 2018), and the multiplicity of the purported flash heating events (Baecker et al., 2017) would further thwart their individual advantage in sodium retention (Jacquet et al., 2015b). Still, recondensation upon cooling could make up for the initial loss (e.g. Alexander et al.,

2000) but the detection of sodium in chondrule olivine cores has suggested that chondrules behaved as essentially closed systems for alkalis below *liquidus* temperatures (Alexander et al., 2008). Barring very high (atmospheric level!) total pressures which could suppress the diffusion of evaporated alkalis away from the chondrules, this would require dust densities in excess of 10^{-3}kg/m^3 , six orders of magnitude above conventional "minimum mass solar nebula" estimates, to allow saturation of the ambient gas in gaseous sodium with a subordinate evaporation fraction per chondrule. This would place chondrule formation in self-gravitating regions, or in definitely "planetary" environments (e.g. Dullemond et al., 2016).

While early chondrule-scale analyses had found no resolvable K isotopic fractionation (Alexander et al., 2000; Alexander and Grossman, 2005), chondrite bulk isotopic measurements have revealed *light* isotope enrichments in K and Rb correlated with the abundance of chondrules (for carbonaceous chondrites), suggestive of recondensation rather than evaporation (Nie et al., 2021; Koefoed et al., 2023). Recondensation has appeared also more graphically suggested by alkali-zoned chondrules, with alkalis concentrated near their margins (e.g. Matsunami et al., 1993; Libourel et al., 2003; Nagahara et al., 2008), even though crystal-melt partitioning or parent body processes were also envisioned (Grossman et al., 2002). The time is thus ripe to revisit the alkali retention problem in a synthetic manner (glass composition, zoning in olivine and mesostases, isotopic constraints), leveraging the data accumulated in the various chondrite groups in the literature. We show that chondrules were definitely open systems for alkalis and revise accordingly the density constraints brought by them.

We will first qualitatively review the cosmochemical evidence for alkali recondensation (from bulk composition, olivine zoning and glass inclusions) in section 2. We will then expose the thermodynamics of this recondensation in section 3, supporting some statements made in advance in the previous section. Yet this, by itself, will not allow conclusions on chondrule-forming conditions, absent a determination of the closure temperature. Section 4 will thus deal with the kinetics of alkali recondensation, in particular the isotopic effects (for multi-isotope alkalis). Only then will section 5 draw and discuss constraints on the astrophysical setting of chondrule formation.

2. Evidence for recondensation

2.1. Data sources

Mesostasis and bulk chondrule data were compiled from the literature for: ordinary (chiefly LL3.0 to LL3.2; DeHart, 1989; Jones, 1990, 1994, 1996; Huang et al., 1996; Grossman et al., 2002; Libourel et al., 2003; Tachibana et al., 2003; Nagahara et al., 2008; Alexander et al., 2008; Kita et al., 2010; Villeneuve, 2010; Jacquet et al., 2015b; Berlin, 2009; Hewins et al., 2012; Grossman et al., 2002), EH (Grossman et al., 1985; Ikeda, 1989; Schneider et al., 2002; Jacquet et al., 2015a; Piani et al., 2016; Douglas-Song et al., 2025), CR (Krot et al., 2004; Mathieu, 2009; Berlin, 2009; Wasson and Rubin, 2010; Ichikawa and Ikeda, 1995; Jacquet et al., 2012; Smith and Jones, 2024), CV (3.0 to 3.1 in the Jacquet and Doisneau (2024) subtypes; Kracher et al., 1985; Kimura and Ikeda, 1997, 1998; Krot et al., 1998; Jacquet et al., 2012), CO (3.0 to 3.2; Rubin and Wasson, 1988; Jones, 1992; Berlin, 2009; Tenner et al., 2013; Friend et al., 2016; Jacquet, 2021), CM (Ikeda, 1983; Olsen, 1983; Kimura et al., 2020), CH (Nakashima et al., 2024), C3-an Acfer 094 (Ushikubo et al., 2012) and Dar al Gani 055 (Varela and Kurat, 2009), C2-an Essebi (Varela and Kurat, 2009), CB_b (Krot et al., 2010), CH/CB_b (Krot et al., 2007). The CM, CO and Acfer 094 data will be grouped in the "CMO" clan (Jacquet, 2022), while "CHB" will refer to CH, CB and Isheyev (which likely derive from a single parent body; e.g. Mahlé et al. (2024)).

2.2. Bulk chondrule compositions

Major and minor lithophile element patterns for bulk chondrules are shown in Fig. 1, for ordinary chondrites, and alkalis are illustrated for different chondrite groups in Fig. 2 and 3. Averages are by types, with an "A" suffix indicating olivine dominating over pyroxene by at least 9:1 (in volume), "B" the contrary relationship, and "AB" the intermediate mineralogies. These are arbitrary divisions in a continuum. There is however a true dichotomy between type I and type II, even though, for ordinary chondrites, IB and IIB chondrules seem to make the connection, and the exact conventional divide in Fe# may vary among authors, as reviewed by Rubin (2024). In carbonaceous chondrites, type II chondrules are essentially restricted to type IIA (there is virtually no Fs content above 10 mol% in the histograms of Wood (1967)), possibly related to their more oxidizing conditions (which promote olivine at the expense of pyroxene; Jacquet and Doisneau (2024)), so the hiatus is clear-cut. In enstatite chondrites, there are none.

The type I chondrules are increasingly volatile- (and alkali-)depleted in the sequence IB-IAB-IA. This is strong evidence for an open system behavior, since pyroxene itself seem to result from interaction with the gas in type I chondrules. Indeed pyroxene is usually concentrated at their margins (Tissandier et al., 2002; Libourel et al., 2006; Barosch et al., 2019) and mesostasis compositions (with anticorrelated SiO_2 and Al_2O_3) reflect dilution by recondensing SiO rather than closed-system subtraction of olivine (Libourel et al., 2006). The silica enrichment of the melt, which did not readily diffuse inward, promoted the formation of pyroxene at the expense of (often poikilitically enclosed) olivine (Libourel et al., 2006; Soulié et al., 2017). So alkalis in particular likely recondensed along with Si (Libourel et al., 2003). Jacquet (2021) showed that volatile elements in (type I) compound chondrule components correlated better (Na/Al has a correlation coefficient of 0.97) than refractory elements, which reflected precursor nugget effects, while the former were buffered by the gaseous environment. The CI-normalized Mn/Na ratio increases in the sequence IA-IAB-IB, presumably because of decreasing equilibration temperature (Sossi et al., 2025), but is lower in EH chondrules than in OC chondrules (0.3 ± 0.1 vs. 1.2 ± 0.2 , one standard error of the mean, $n=33$ and 46 respectively), reflecting lower oxygen fugacity in the former (Sossi et al., 2025).

For type II chondrules, their near-chondritic bulk compositions provide less evidence in themselves for open system, even though the IIB and IIAB are somewhat volatile-depleted (possibly owing to less oxidizing conditions, see Jacquet et al. (2015b) and the next sections). At any rate, the Na/Al correlation previously reported for reconstructed 2D bulks should no longer be interpreted in terms of an albite or oligoclase precursor (in a closed-system scenario, also ; Hewins, 1991; Jacquet et al., 2015b). Mesostasis itself, which is the main carrier of Na and Al , shows no such correlation (e.g. Hewins et al., 2012), and that observed for reconstructed bulks is then likely an artifact of varying proportions of mesostases appearing in the 2D sections analyzed (Hezel and Kießwetter, 2010). It is just a matter of coincidence that the CI chondritic Na/Al ratio (0.68; Lodders (2003)) is close to that of albite—indeed, feldspar in equilibrated ordinary chondrites, which is the main carrier of both Na and Al , has an oligoclase composition (e.g. $\text{Ab}_{86}\text{An}_{10}\text{Or}_4$ for equilibrated LL chondrites, hence a Na/Al ratio of 0.78; (Brearley and Jones, 1998)). Interestingly, most type II (in particular IIA) chondrules in ordinary chondrites show suprachondritic K/Al ratios (with an average CI-normalized K/Al of 1.3 ± 0.1 , one standard error of the mean, $n=96$; Fig. 3, 7), which

cannot be accounted for by incomplete recondensation in a closed chondritic reservoir. Unless K-depleted type II chondrules were underrepresented in our compilation, this suggests an influx of K, e.g. lost from type I chondrules if formed nearby (e.g. Ruzicka, 2012).

2.3. Olivine zoning

Alexander et al. (2008) claimed a closed-system behavior for Na below liquidus temperatures because they detected Na even in the core of olivine crystals. Forsteritic relicts grains (e.g. Pinto et al., 2024) concealed by Fe-Mg interdiffusion in back-scattered electron images, as speculated by Jacquet et al. (2024), would not be a solution, since those visible are distinctly Na-depleted compared to surrounding host olivine (Alexander et al., 2007). Alexander et al. (2008) could fit the zoning profiles with a fractional crystallization model (i.e. with negligible diffusion). This, in fact, holds for type II chondrules rather than type I chondrules which show little zoning (Fig. 4)—and for which a closed system would imply *higher* dust densities, despite their lower recorded oxygen fugacity, because of their higher liquidus temperatures (Alexander et al., 2008).

However, this approach neglected the positive correlation of the olivine/melt Na partition coefficient for Na with FeO (Mathieu, 2009)¹. If one sticks to the fractional crystallization hypothesis, one must allow for a post-liquidus loss of half of the Na from type II chondrules, followed, for type IIAB, by more or less complete recovery (Hewins et al., 2012). This could evoke impact plume expansion scenarios, where cooling is counteracted by the density decrease for Na retention (Dullemond et al., 2016). Yet, as mentioned in the previous subsection, type IIA chondrules seem to have lost overall *less* Na (with respect to a chondritic precursor, when normalized to refractory Al), on average, than type IIAB chondrules.

In fact, crystallizing olivine may not have been closed to diffusion. Diffusivities for Na are of the same order of magnitude than for other minor elements (Cr, Mn, Ca, Fe-Mg) in the experiments of Spandler and O’Neill (2009), around $10^{-15} \text{ m}^2/\text{s}$ at 1300°C , even though profiles through forsteritic relict grains suggest it is somewhat slower than the others (Alexander et al.,

¹We may neglect contrary claims by Jacquet et al. (2015b) based on the activity coefficient of Na in the melt, for this is obviously not the only factor in the partition coefficient when writing the action mass law for the substitution reaction, and should thus not supersede the empirical evidence brought by Mathieu (2009).

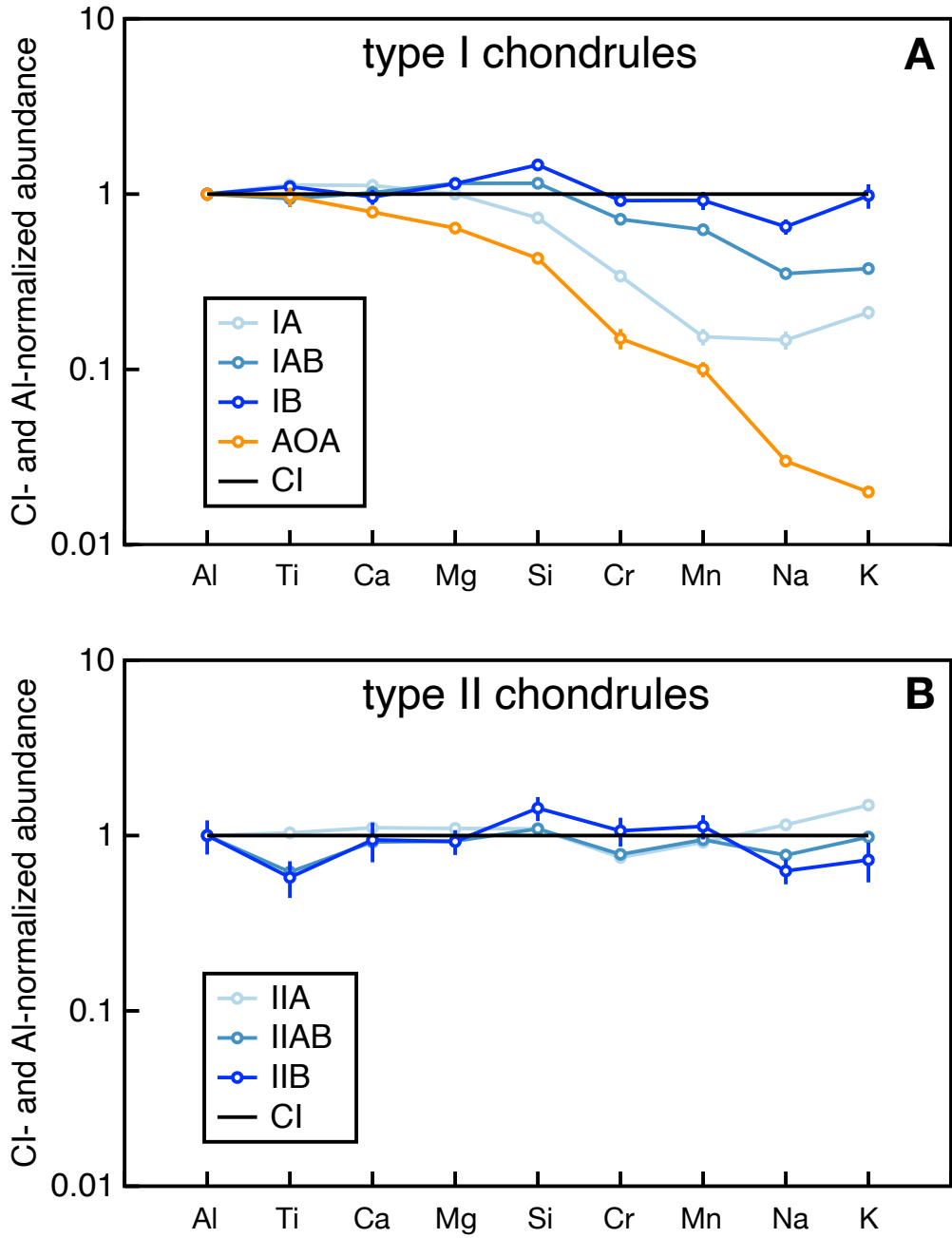


Figure 1: Abundance patterns for elements arranged in order of increasing volatility for different types of chondrules in ordinary chondrites (type I and II in panels A and B respectively). The numbers of averaged chondrules were 19 (IA), 17 (IAB), 9 (IB), 7 (IIB), 45 (IIAB), 41 (IIA). Error bars are one standard error of the mean. The profile for amoeboid olivine aggregates (AOA; Ruzicka et al., 2012) is also shown.

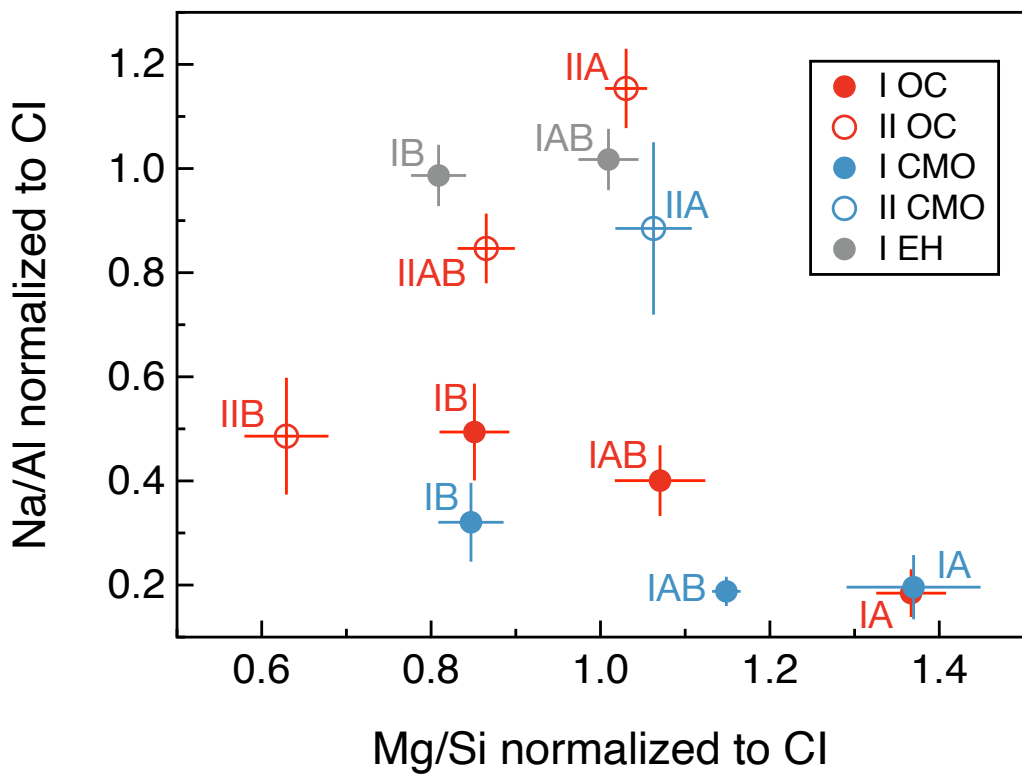


Figure 2: Mean Na/Al versus Mg/Si ratios for different chondrule types in ordinary, enstatite and CMO chondrites. Error bars are one standard error of the mean. The numbers of averaged chondrules were the same as Fig. 1 for OCs, and, for CMO, 70 (IAB), 18 (IB), 8 (IIA), and for EH, 17 (IAB) and 19 (IB).

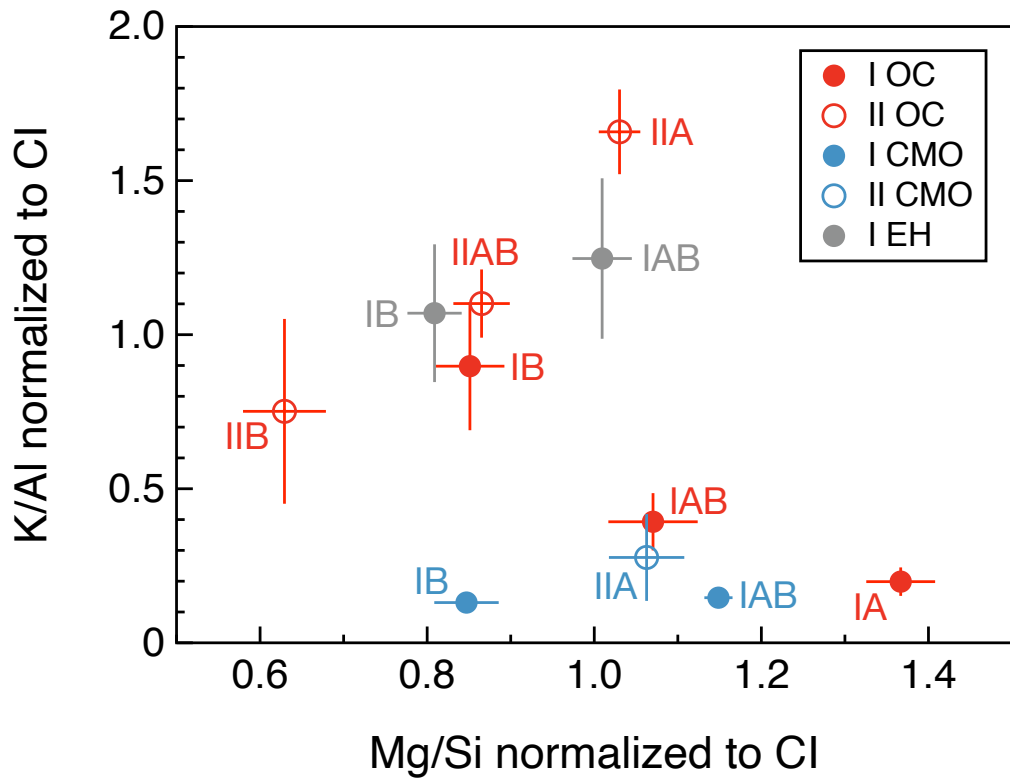


Figure 3: Mean K/Al versus Mg/Si ratios for different chondrule types in ordinary, enstatite and CMO chondrites. Error bars are one standard error of the mean. Same numbers of averaged chondrules as Fig. 2.

2007). For reference, diffusivities of $10^{-15} \text{ m}^2/\text{s}$ would allow core values within one order of magnitude of the rim within a few hours for grains of a few tens of μm (Crank, 1975). Since Miyamoto et al. (2009) did find varying degrees of diffusional modifications of Fe-Mg zoning profiles in Semarkona type II chondrules, Na should have significantly diffused as well. Zoning is stronger for Na than for other elements (Fig. 4), consistent with more sluggish diffusion and/or more contrasted original profile (e.g. Na-free original cores). Zoning is nevertheless less pronounced for the most fayalitic olivines, perhaps as a result of increased diffusivity for higher Fa contents and/or oxygen fugacities (as seen for other elements, e.g. Chakraborty (2010)). So we may be witnessing incipient diffusion of Na from olivine margins toward the core, which was more efficient for type I chondrules, closer to batch crystallization (Jacquet et al., 2015b, 2012). More direct evidence for diffusion is given by another alkali element, Li, with isotopically lighter and elementally lower compositions in the center of olivine crystals (Neukampf et al., in press), which results from the 5 % higher diffusivity (e.g. Chakraborty, 2010) of ${}^6\text{Li}$ compared to ${}^7\text{Li}$. Indeed, had diffusion been negligible, the isotopic fractionation (relative to the gaseous reservoir) in olivine cores would be negligible owing to rapid gas-melt equilibration at high temperatures (see section 4).

2.4. Glass inclusions

The olivine zoning profiles are thus equivocal at best, but olivine-hosted glass inclusions offer a clear message. Indeed, they represent melt trapped earlier than that solidified as the mesostasis interstitial to the phenocrysts (e.g. Varela and Kurat, 2009; Florentin et al., 2017). The compositional ratio of choice is Na/Al, for it is insensitive to mineral crystallization after trapping (since both Na and Al are very incompatible elements in olivine and pyroxene) and Al is refractory and thus near closed-system behavior. We can see in Fig. 5 that glass inclusions are systematically depleted in Na (often below detection) compared to the mesostasis, even (if to a lesser extent) in type II chondrules. There is a minor Na-rich glass inclusion population in CR chondrites (Varela et al., 2002), which may have been trapped relatively late, or even be connected in the third dimension to the mesostasis, like the (indeed more Na-rich) "neck inclusions" in the CV chondrite Kaba (Varela et al., 2005).

To be sure, Florentin et al. (2017) reported that most glass inclusions in Allende are Na-rich but these are likely the result of metasomatism on the parent body. Indeed, although most Na-enriched mesostases are devitrified

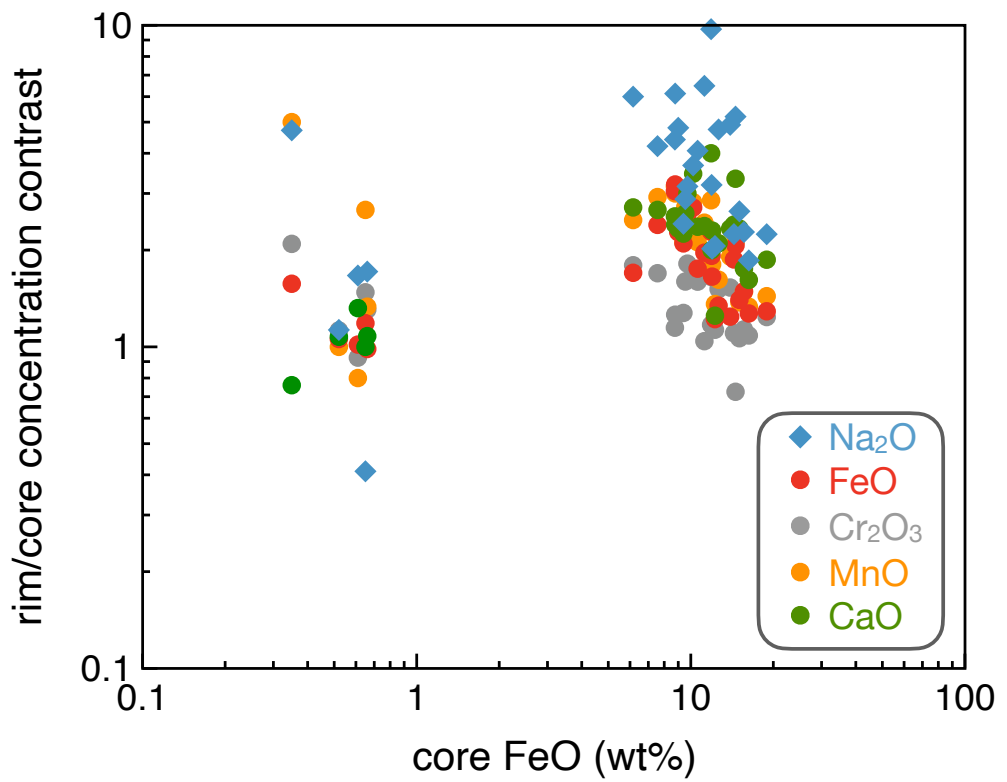


Figure 4: Minor element concentration ratio between rim and core olivine in ordinary chondrites (Alexander et al., 2008; Hewins et al., 2012), as a function of core FeO content.

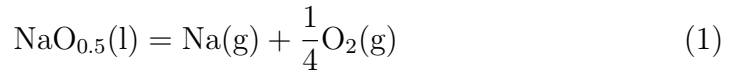
(Ikeda and Kimura, 1995; Kimura and Ikeda, 1995), closer observations indicate that Na enrichment preceded devitrification (Ikeda and Kimura, 1996). The fact that heating experiments on Allende glass inclusions by Florentin et al. (2017) caused no Na loss is certainly no contradiction, since heating was the cause of metasomatism. Chondrites heated below metamorphic grade M0.2 (equivalent to subtype 3.2), which is that of Allende in the Jacquet and Doisneau (2024) classification, uniformly show mostly Na-depleted glass inclusions.

These evidence that earlier (higher-temperature) melts, and thus chondrules as wholes, were alkali-poorer than the later ones. Melts were thus open both to interaction with the gas and silicate subtraction. This is not unlike the "Primary Liquid Condensation model" of Varela and Kurat (2009), although evidence for solid precursors (e.g. Krot et al., 2006; Marrocchi et al., 2018, 2019; Piralla et al., 2021; Misawa and Nakamura, 1988; Jacquet and Marrocchi, 2017; Schneider et al., 2020) suggest chondrules were not *wholly* produced by condensation. The chondritic ratios of refractory lithophile elements in glasses put forward by Varela and Kurat (2009) simply reflect their incompatibility in the other phases (so that they represent bulk precursor ratios, as the refractory elements in question hardly evaporated from the chondrules). At any rate, chondrules of both types I and II were open systems in alkalis.

3. Thermodynamics of alkali condensation

It is time to get more quantitative by modelling the equilibrium between the gas and chondrule melt. We consider a chondrule composed of a silicate liquid (with a mass fraction x_l , which may depend on time) and other phases (e.g. silicate crystals, possibly with melt inclusions) which are negligible carriers of the alkali budget and thus not further modelled here (however useful their trace amounts may be to track condensation history as discussed in the previous section). For simplicity, we focus on sodium, but any notation to follow with an "Na" subscript may be adapted for another alkali, and thermodynamic evaluations for them are given in Appendix B. Table 1 recapitulates the main symbols used in the text.

We call K_{Na} the equilibrium constant of the reaction



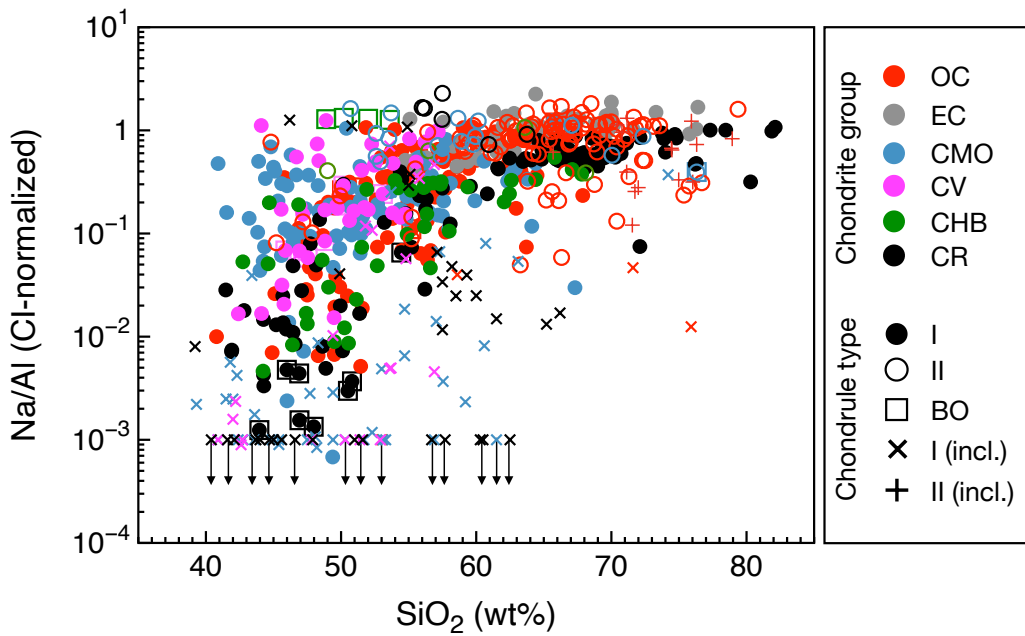


Figure 5: Mesostasis/glass Na/Al vs. SiO₂ contents for chondrules in different chondrite groups. Colors code the groups and symbol shapes/filling code the petrographic setting. In particular, open circles represent type II chondrules and crosses refer to olivine-hosted glass inclusions ("incl.") from CR (Varela et al., 2002), C3-an Acfer 094 (Varela and Kurat, 2009), CM (Fuchs et al., 1973; Desnoyers, 1980; Varela and Kurat, 2009; Florentin et al., 2017), CV (Varela et al., 2005; Varela and Kurat, 2009), LL (Varela and Kurat, 2009; Hewins et al., 2012) chondrites. Values below detection are reported as upper limits at 10⁻³.

Table 1: Table of the main symbols used in the main text (excluding appendices or footnotes). Symbols may be further subscripted by isotopes (i, j) or element, or phases ("chd"=chondrule, "g"=gas), not all possibilities of which are indicated.

Symbol	Meaning
α	condensation coefficient
γ	surface tension of molten chondrule
$\gamma_{EO_{0.5}}$	activity coefficient
$\delta^{i/j} E$	relative deviation of ${}^i E / {}^j E$ to the standard
η	melt viscosity
Λ	optical basicity
ϕ	crystal volume fraction in chondrule
ρ_p	chondrule density (as a swarm)
ρ_s	internal chondrule density
τ_{eff}	equilibration timescale of the gas with the chondrules
Ω_E	diffusion factor of element E
a	chondrule radius
$E_{\text{chd/g}}$	equilibrium budget ratio (i.e. $f_j / (1 - f_j)$) of element E
$(E/F)_{\text{chd/g}}$	equilibrium ratio of E/F ratios in chondrules and gas
Fa	fayalite content in chondrule olivine (=Fe/(Fe+Mg))
f_j	condensed fraction of isotope j
f_{O_2}	oxygen fugacity (dimensionless, i.e. P_{O_2} / P_0)
$f_{O_2, \text{IW}}$	oxygen fugacity of the Iron-Wüstite (IW) buffer
K_{Na}	evaporation reaction constant for Na
MDF	mass-dependent fractionation per relative mass difference
m_{Na}	mass of Na atom
m_l	mean molecular weight in melt
m_p	chondrule mass
Na_l	mass fraction of Na in melt
N_i	total atom number density of isotope ${}^i E$
n_i	number density of gaseous isotopolog ${}^i E$
n_p	chondrule number density
P_{Na}	partial pressure of Na
P_0	standard pressure (1 bar)
t_{rec}	equilibration (recondensation) timescale of a single chondrule with the gas
T_{Fa}	numerator in the Arrhenian dependence of f_{O_2} as a function of Fa
T_{Na}	numerator in the Arrhenian dependence of K_{Na}
T_{IW}	numerator in the Arrhenian dependence of $f_{O_2, \text{IW}}$
T_{rec}	numerator in the Arrhenian dependence of t_{rec} , $E_{\text{chd/g}}$
v_T	mean thermal velocity
x_l	melt mass fraction in chondrule
X_{Na}	number of Na atoms in the chondrule of interest
$X_{\text{buf,Na}}$	value of X_{Na} buffered by the ambient n_{Na}
w	shape-dependent parameter in the expression of D_{eff}

Unless otherwise noted, the free enthalpies of chemical reactions were fitted to NIST-JANAF thermodynamical data available online (Stull and Prophet, 1971). Between 1200 and 3000 K, a satisfactory fit is:

$$K_{\text{Na}} = 9.5 \times 10^5 \exp\left(-\frac{T_{\text{Na}}}{T}\right) \quad (2)$$

with $T_{\text{Na}} = 30686$ K (essentially the enthalpy of the above reaction in standard conditions, divided by the Boltzmann constant k_B). This is 0.0103 at 1400°C (that is 1673 K) which will serve as our reference temperature because most Na solubility experiments conducted or compiled by Mathieu (2009) were at this temperature.

From the action mass law, we can derive:

$$\text{Na}_l = \frac{P_{\text{Na}} f_{O_2}^{1/4} m_{\text{Na}}}{P_0 K_{\text{Na}} \gamma_{\text{NaO}_{0.5}} m_l} \quad (3)$$

with P_{Na} the partial pressure of Na, f_{O_2} the oxygen fugacity, $P_0 = 1\text{bar}$ the standard pressure, m_{Na} the mass of the Na atom, m_l the mean "molecular" (oxide) mass in the melt, $\gamma_{\text{NaO}_{0.5}}$ the activity coefficient of $\text{NaO}_{0.5}$. The calculation of the activity coefficients is detailed in Appendix A. Suffice it to say that it is an increasing function of the optical basicity Λ which anticorrelates with silica content. In other words, sodium solubility correlates with silica.

We may reason in terms of the chondrule bulk Na concentration $\text{Na}_{\text{chd}} = \text{Na}_l x_l^2$. Averaging over all chondrules, and noting ρ_p their local density, we obtain the ratio of Na budgets in the chondrules to that in the gas:

$$\text{Na}_{\text{chd/g}} = \frac{k_B T f_{O_2}^{1/4} \rho_p}{P_0 K_{\text{Na}}} \left\langle \frac{x_l}{\gamma_{\text{NaO}_{0.5}} m_l} \right\rangle \quad (4)$$

$$= 2 \times 10^{-3} \left(\frac{\langle x_l / (\gamma_{\text{NaO}_{0.5}} m_l) \rangle}{40 \text{ amu}^{-1}} \right) \left(\frac{\rho_p}{10^{-6} \text{ kg/m}^3} \right) \left(\frac{f_{O_2}}{f_{O_2, \text{IW}}} \right)^{1/4} \left(\frac{1673 \text{ K}}{T} \right)^{0.49} \exp \left(\left(T_{\text{Na}} - \frac{T_{\text{IW}}}{4} \right) \left(\frac{1}{T} - \frac{1}{1673 \text{ K}} \right) \right) \quad (5)$$

²This breaks down for Li, with olivine/melt partition coefficients of 0.13-0.35 (Spandler and O'Neill, 2009), in which case we would need to replace x_l by $x_l + \sum_i x_i D_{i/l}$ with x_i the mass fraction of crystalline phase i and $D_{i/l}$ its partition coefficient with the liquid.

where $\langle \dots \rangle$ denotes chondrule mass-weighted averaging, k_B the Boltzmann constant, and

$$f_{O_2, IW} = 3 \times 10^7 \left(\frac{1673K}{T} \right)^{2.03} \exp \left(-\frac{T_{IW}}{T} \right) \quad (6)$$

the oxygen fugacity of the iron-wüstite (IW) buffer, with $T_{IW} = 66261$ K, for total pressures much lower than atmospheric (Wolf et al., 2023). This normalization is chosen because $f_{O_2}/f_{O_2, IW}$ weakly varies with temperature in condensation calculations (Mokhtari and Bourdon, 2026). The normalizing value for $x_l/(\gamma_{NaO_{0.5}}(1673K)m_l)$ corresponds to the average of type I OC chondrules (38 ± 5 amu $^{-1}$ vs. 66 ± 5 amu $^{-1}$ for type II and 50 ± 4 and 28 ± 5 amu $^{-1}$ in EH and CMO respectively; \pm one standard error of the mean, $n=28, 56, 36, 28$, respectively).

The compositional evolution of the chondrule during cooling would have had little effect on the right-hand-side of equation 4. Indeed, although crystallization would have reduced x_l , $\gamma_{NaO_{0.5}}(1673K)$ would have decreased too because of increasing silica content in the melt. For chondrules with both bulk and mesostasis data, $x_l/(\gamma_{NaO_{0.5}}(1673K)m_l)$ of the bulk is higher than the mesostasis by an average (\pm standard error of the mean) factor of 4.5 ± 0.9 ($n=28$) for type I and 2.9 ± 0.7 ($n=55$) for type II chondrules in OC. Yet surely the actual peak temperature composition of the (partially evaporated) chondrules was more refractory than the present-day bulk composition, and would thus have had a higher optical basicity and hence $\gamma_{NaO_{0.5}}(1673K)$, reducing the above factor.

Thus, the explicit temperature dependence would be the main control on $Na_{chd/g}$, and it is a strong one. Indeed $Na_{chd/g} \propto \exp(T_{rec,Na}/T)$ with

$$T_{rec,Na} = T_{Na} - \frac{T_{IW}}{4} - (1673 \text{ K}) \ln \gamma_{NaO_{0.5}}(1673 \text{ K}) = 29619 \text{ K} \quad (7)$$

where the numerical evaluation assumes $\gamma_{NaO_{0.5}}(1673K) = 10^{-4}$. At 1400 °C, the "thermal e-folding" $|dT/d\ln Na_{chd/g}| \approx T^2/T_{rec,Na}$ is about 100 K. So one or a few hundred degrees difference between melt trapping in an olivine crystal and closure of mesostasis would account for the Na-depletion in glass inclusions. Only a competing order-of-magnitude decrease of ρ_p could reverse the effect, as in a plume expansion scenario (Dullemond et al., 2016).

The strong temperature dependence also means that once the constraint that Na was quantitatively condensed at liquidus (Alexander et al., 2008) is

eliminated, the density constraints can be alleviated. All normalizations of equation 4 equal (with a uniform $\gamma_{\text{NaO}_{0.5}}(1673\text{K}) = 10^{-4}$), the half-condensation temperature of Na (i.e. where $\text{Na}_{\text{chd/g}} = 1$) is: 1120, 1230, 1360 K for $\rho_p = 10^{-7}, 10^{-6}, 10^{-5} \text{ kg/m}^3$, respectively (this becomes 1030, 1120, 1230 K at IW-4, i.e. $\log_{10}(f_{O_2}/f_{O_2,\text{IW}}) = -4$). These are higher than "canonical" values, e.g. 958 K for a solar gas at 10^{-3} bar for Lodders (2003), which would correspond to more reducing conditions (IW-6; Ebel and Grossman (2000)) and a relatively low $\rho_p \approx 10^{-7} \text{ kg/m}^3$.

The higher alkali content of type II chondrules compared to type I chondrules may stem from their higher f_{O_2} , but possibly also from higher absolute ρ_p . Since $f_{O_2} \propto (O/H - C/H)^{1/2}$ (e.g. Grossman et al., 2008), that is, proportional to the square root of the solid/gas ratio, both might have covaried, e.g. for a constant background gas density.

The general positive correlation of alkalis with SiO_2 (Fig. 6, 7) of type I chondrule mesotases also supports recondensation. Indeed, alkali solubility is positively correlated with silica content, via the activity coefficients (Libourel et al., 2003; Mathieu, 2009). However, Na varies more steeply than $\gamma_{\text{NaO}_{0.5}}^{-1}$ (Fig. 8) except when leveling off near chondritic Al-normalized values. In no chondrite group are we simply witnessing a population of chondrules equilibrated with the same gas, at the same temperature. Since SiO_2 contents increased as a result of SiO solubilization (Libourel et al., 2006), the chondrules seem to sample an array of different closure temperatures, or time-temperature histories. We thus need to investigate the kinetics of recondensation.

4. Kinetics of recondensation

4.1. Hertz-Knudsen equation

Let X_{Na} be the number of Na atoms of the chondrule of interest. Provided the said chondrule is much smaller than the mean molecular mean free path of the gas, it obeys the Hertz-Knudsen equation (e.g. Richter, 2004; Richter et al., 2009; Fedkin et al., 2006):

$$\frac{dX_{\text{Na}}}{dt} = \pi a^2 (1 - \phi) \alpha_{\text{Na}} (n_{\text{Na}} - n_{\text{Na,sat}}) v_{\text{T,Na}} = \frac{X_{\text{buf,Na}} - X_{\text{Na}}}{t_{\text{rec,Na}}} \quad (8)$$

with α_{Na} the condensation coefficient (identified with the evaporation coefficient), n_{Na} the concentration of gaseous Na, $n_{\text{Na,sat}}$ its saturation value (in

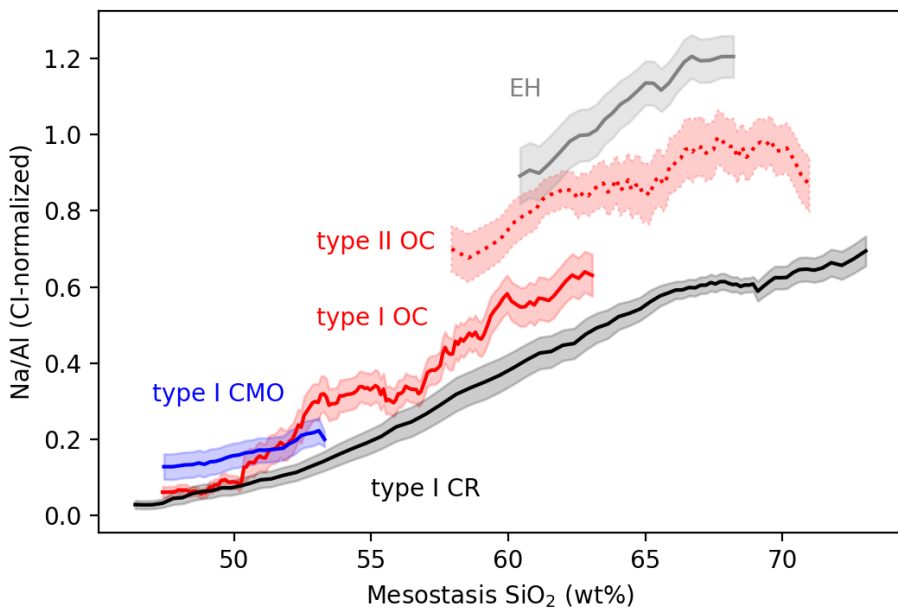


Figure 6: Rolling averages of Na/Al (CI-normalized) for mesostasis data (30 averaged at a time) ordered by SiO₂ content (\pm one standard error of the mean shaded). As explained in subsection 2.4, the ratio Na/Al allows to gauge gain of Na, as both Na and Al are incompatible and Al is refractory.

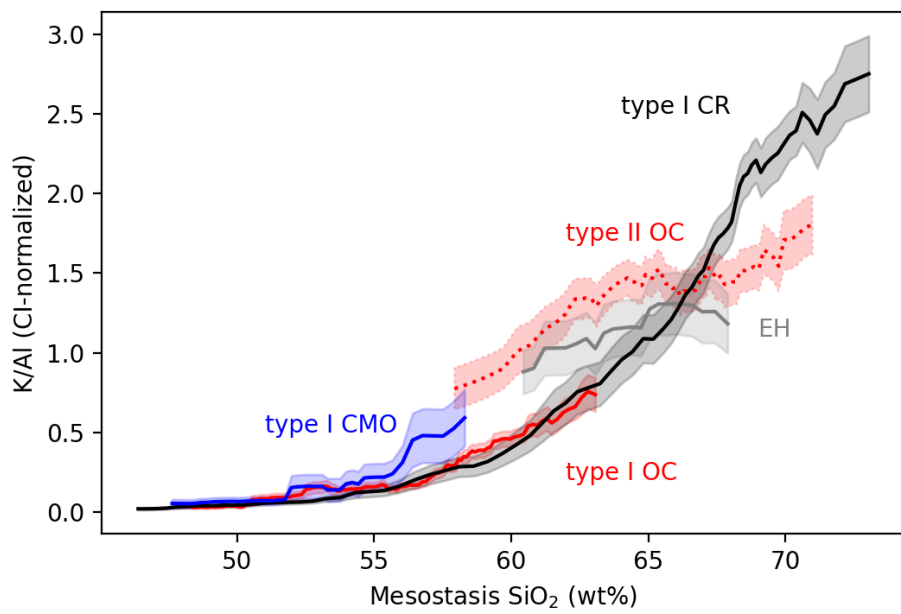


Figure 7: Rolling averages of K/Al (CI-normalized) for mesostasis data (30 averaged at a time) ordered by SiO₂ content (\pm one standard error of the mean shaded).

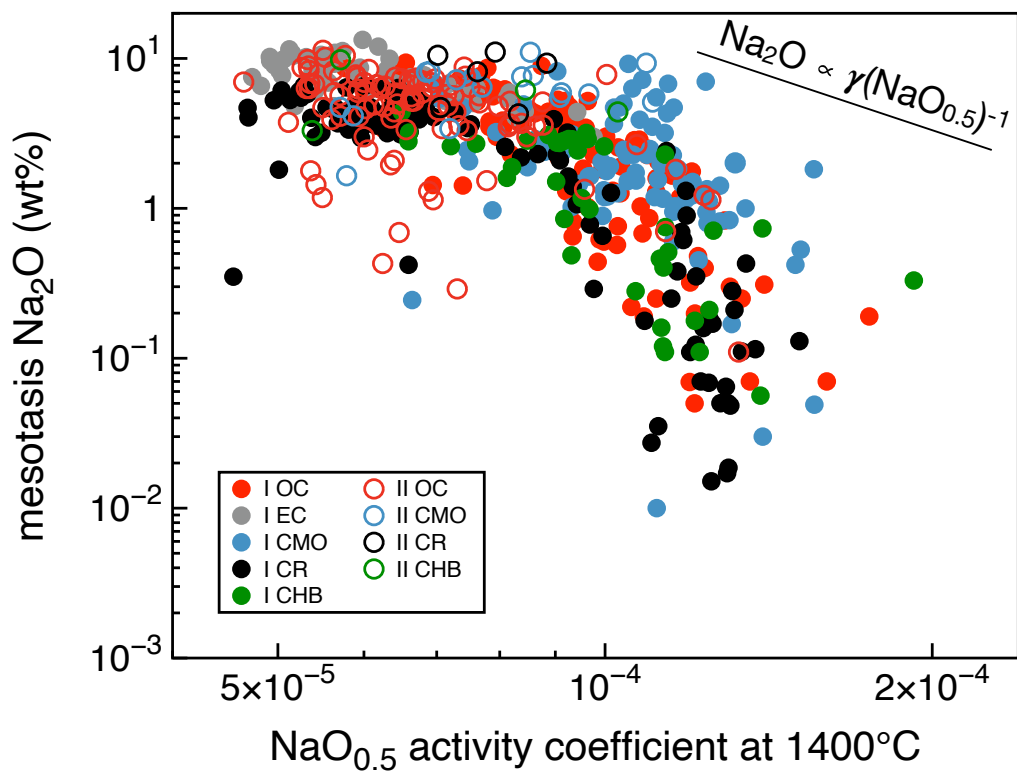


Figure 8: Mesostasis Na_2O vs. activity coefficient $\gamma_{\text{NaO}_{0.5}}$ in the Henry domain at 1400°C . The slope of a dependence $\text{Na}_2\text{O} \propto \gamma_{\text{NaO}_{0.5}}^{-1}$ which would apply for constant T and partial pressures of Na and O_2 is also shown for comparison.

equilibrium with the actual melt composition), $v_{T,\text{Na}} = \sqrt{8k_B T / (\pi m_{\text{Na}})}$ the thermal speed of Na gas molecules. The $(1 - \phi)$ factor, with ϕ the volume fraction of crystals, is a rough estimate of the fraction of surface of the chondrule occupied by melt (on the one hand, crystals are more concentrated near the surface either as olivine palissades (Libourel and Portail, 2018) or pyroxene rims (Libourel et al., 2006), inhibiting exchange (Ozawa and Nagahara, 2001), but on the other hand melt may wet them). We have coined the recondensation timescale

$$\begin{aligned} t_{\text{rec,Na}} &= \frac{\rho_s a \sqrt{2\pi m_{\text{Na}} k_B T} f_{O_2}^{1/4} x_l}{3P_0 K_{\text{Na}} \alpha_{\text{Na}} m_l \gamma_{\text{NaO}_{0.5}} (1 - \phi)} \quad (9) \\ &= 22 \text{ s} \left(\frac{\rho_s a}{1 \text{ kg/m}^2} \right) \left(\frac{0.1}{\alpha_{\text{Na}}} \right) \left(\frac{x_l / (\gamma_{\text{NaO}_{0.5}}(1673\text{K}) m_l)}{40 \text{ amu}^{-1}} \right) \left(\frac{f_{O_2}}{f_{O_2,\text{IW}}} \right)^{1/4} \\ &\quad \left(\frac{T}{1673\text{K}} \right)^{0.01} \exp \left(T_{\text{rec,Na}} \left(\frac{1}{T} - \frac{1}{1673\text{K}} \right) \right) (1 - \phi)^{-1} \end{aligned}$$

with ρ_s the density of the chondrule and $X_{\text{buf,Na}}$ the value of X_{Na} buffered by the ambient gas composition. The normalizing value of α_{Na} is inspired from Fedkin et al. (2006) who found 0.26 in vacuum and 0.042 under 9 Pa H₂. The $f_{O_2}^{1/4}$ dependence was experimentally confirmed by Tsuchiyama et al. (1981).

$t_{\text{rec,Na}}$, which is also an evaporation timescale, is short for typical liquidus temperatures. We calculate 0.3 s at 1960 K and IW-3 for our usual normalizations (with $\gamma_{\text{NaO}_{0.5}}(1673\text{K}) = 10^{-4}$), comparable to the 0.5 s convergence timescale quoted by Fedkin and Grossman (2013) for their type I model chondrule composition. No precursor alkali content should thus survive the heating. Indeed:

$$\begin{aligned} X_{\text{Na}} &= X_{\text{buf,Na}} - \int_0^t \exp \left(- \int_{t'}^t \frac{dt''}{t_{\text{rec,Na}}} \right) \frac{dX_{\text{buf,Na}}}{dt} dt' \\ &\quad + (X_{\text{Na}}(0) - X_{\text{buf,Na}}(0)) \exp \left(- \int_0^t \frac{dt'}{t_{\text{rec,Na}}} \right) \\ &\approx X_{\text{buf,Na}} - t_{\text{rec,Na}} \frac{dX_{\text{buf,Na}}}{dt} \quad (10) \end{aligned}$$

where the approximation assumes that $t_{\text{rec,Na}}$ is shorter than both the elapsed time (henceforth the *limit of forgotten beginnings*) and the timescale of variation of $X_{\text{buf,Na}}$ —or more precisely for the latter condition, that:

$$\frac{d}{dt} \left(t_{\text{rec,Na}} \frac{dX_{\text{buf,Na}}}{dt} \right) / \frac{dX_{\text{buf,Na}}}{dt} \ll 1 \quad (11)$$

However, as the temperature decreases, the lag time t_{rec} increases and ultimately overtakes the cooling timescale, effectively stopping the alkali influx.

4.2. Isotopic fractionation

The recondensation timescale t_{rec} being shorter for lighter isotopologs (for alkalis other than Na which are multi-isotopic in nature), we would expect an excess of lighter isotopes in the chondrule. Indeed, by plugging in the relevant Hertz-Knudsen equations, the isotopic ratio for two isotopes i and j of an element E evolves as:

$$\frac{d}{dt} \left(\frac{X_i}{X_j} \right) = \frac{1 + \sqrt{\frac{m_i}{m_j}} \alpha_{\text{chd-g}}^{i/j} \left(\frac{X_{\text{buf,j}}}{X_j} - 1 \right)}{t_{\text{rec,i}}} \left[\frac{\alpha_{\text{chd-g}}^{i/j} n_i / n_j}{1 + \left(\sqrt{\frac{m_i}{m_j}} \alpha_{\text{chd-g}}^{i/j} - 1 \right) \left(1 - \frac{X_j}{X_{\text{buf,j}}} \right)} - \frac{X_i}{X_j} \right] \quad (12)$$

with $\alpha_{\text{chd-g}}^{i/j}$ the chondrule/gas (equilibrium) fractionation coefficient, where we have ignored any mass-dependence of the condensation coefficients (Zhang et al., 2021). Hence, X_i/X_j should converge rapidly toward the first term between the brackets (so long as inequation 11 applies). In terms of the relative deviations of relative deviation of the ${}^iE/{}^jE$ ratio to a terrestrial standard, we would have:

$$\begin{aligned} \delta^{i/j} E_{\text{chd}} - \delta^{i/j} E_{\text{g}} &\approx \frac{X_i n_j}{X_j n_i} - 1 \\ &\approx \alpha_{\text{chd-g}}^{i/j} - 1 + \left(\sqrt{\frac{m_i}{m_j}} - 1 \right) \left(\frac{X_j}{X_{\text{buf,j}}} - 1 \right) \\ &\approx - \left(\sqrt{\frac{m_i}{m_j}} - 1 \right) t_{\text{rec,j}} \frac{d \ln X_{\text{buf,j}}}{dt} \end{aligned} \quad (13)$$

Since $X_j/X_{\text{buf,j}} = n_{\text{sat,j}}/n_j$, the second form amounts to equation 31 of Richter (2004) when equilibrium fractionation is neglected ($\alpha_{\text{chd-g}}^{i/j} \approx 1$), as done in the third form³.

³From the values quoted by Zhang et al. (2021), the correction to the MDF (defined later), $(1 - f_j)(\alpha_{\text{chd-g}}^{i/j} - 1)/(m_i/m_j - 1)$, would be a positive MDF shift of 0.001 – 0.002

Assuming the whole chondrule-forming region (CFR) comprises a population of identical-composition chondrules, in addition to the gas, with overall concentration (condensed+gaseous) N_i and N_j for the isotopes in question, we have:

$$\delta^{i/j} E_{\text{chd}} - \delta^{i/j} E_{\text{CFR}} = - (1 - f_j) \left(\sqrt{\frac{m_i}{m_j}} - 1 \right) \langle t_{\text{rec},j} \rangle \frac{d \ln}{dt} \left(\frac{N_j/n_p}{E_{\text{chd/g}}^{-1} + 1} \right) \quad (14)$$

with f_j the recondensed fraction of isotope j (essentially that of the element E as a whole) and n_p the number density of chondrules. Assuming N_j/n_p to be constant (which would still allow for expansion of the coupled gas+chondrule cloud), and using

$$\frac{t_{\text{rec},j}}{E_{\text{chd/g}}} = \frac{1 - f_j}{f_j} t_{\text{rec},j} = \frac{4\rho_s a}{3\rho_p v_{T,j} \alpha_j (1 - \phi)} \equiv \tau_{\text{eff},j}, \quad (15)$$

we can express the mass-dependent fractionation per relative mass difference MDF as:

$$\begin{aligned} \text{MDF} &\equiv \frac{\delta^{i/j} E_{\text{chd}} - \delta^{i/j} E_{\text{CFR}}}{m_i/m_j - 1} \\ &= -\frac{\tau_{\text{eff},j}}{2} f_j (1 - f_j) \frac{d \ln E_{\text{chd/g}}}{dt} \\ &= -0.02 \left(\frac{f_j (1 - f_j)}{10^{-1}} \right) \left(\frac{\langle \rho_s a \rangle}{1 \text{ kg/m}^2} \right) \left(\frac{10^{-6} \text{ kg/m}^3}{\rho_p} \right) \left(\frac{0.1}{\alpha_j} \right) (1 - \phi)^{-1} \\ &\quad \left(\frac{m_j}{39 \text{ amu}} \right)^{1/2} \left(\frac{1500 \text{ K}}{T} \right)^{1/2} \left(\frac{100 \text{ K}}{|dT/d \ln E_{\text{chd/g}}|} \right) \left(\frac{|dT/dt|}{10 \text{ K/h}} \right) \end{aligned} \quad (16)$$

The parabolic $f_j (1 - f_j)$ dependence reproduces those calculated by Nie et al. (2021) for constant cooling rates (if skewed past $f_j = 1/2$ by the increase of $|d \ln E_{\text{chd/g}}/dT|$). This comes about because for $f_j \ll 1$, equilibration is efficient and kinetic mass fractionation thus minimal, while for f_j approaching 1, the chondrules have essentially recovered all the E budget of the reservoir, erasing any isotopic fractionation relative to it. As in

for both K and Rb at 1400 °C (with a dependence $\propto 1/T^2$) in the limit $f_j \ll 1$. This is subordinate compared to the MDF values tabulated in 2, which are dominated by the (negative) kinetic contribution.

Richter (2004), we see that the MDF has a small absolute value so long as the cooling timescale ($\sim dt/d\ln E_{\text{chd/g}}$) is long compared to the gas equilibration timescale τ_{eff} .

Carbonaceous chondrite chondrule MDF values are calculated for alkali and other moderately volatile elements in table 2. We assume that the (mass-dependent) isotopic composition of the reservoir prior to chondrule formation was that of CI chondrites. This neglects nucleosynthetic contributions to mass-dependent isotopic variations. The K nucleosynthetic anomaly variations in $\epsilon^{40}\text{K} \approx \delta^{40/39}\text{K} - 0.5\delta^{41/39}\text{K}$ are of order 0.1 ‰ (Nie et al., 2023), but, if indeed ascribable to type II supernovae, are essentially due to ^{40}K : for the yields adopted by Nie et al. (2023), fresh supernova ejecta should have $\delta^{41/39}\text{K}/\epsilon^{40}\text{K} = 10^{-2}$ so their admixtures would not appreciably affect the $\delta^{41/39}\text{K}$. Likewise, mass-independent nucleosynthetic anomalies in Zn vary by less than 0.01 ‰ among bulk CCs (Savage et al., 2022) and thus suggest similar inherited variations for mass-dependent ratios (prior to evaporation), negligible compared to the fraction of permil effects observed. The Li isotopic variations are also limited among bulk carbonaceous (or unequilibrated ordinary) chondrites (Seitz et al., 2007).

The calculated MDF have similar orders of magnitude for the different moderately volatile elements. Indeed, so long as we deal with trace elements dissolving in some phase, the mathematical treatment above should be similar (e.g. Lodders et al., 2025), although relevant gas fugacities (other than that of the element-containing species, e.g. O_2 here) may differ. The temperature dependence the chondrule/gas budget ratios should be largely dictated by the enthalpy of the condensation reactions, which have similar orders of magnitude (hundreds of kJ/mol; e.g. table 5 of Sossi et al. (2019); Table B.6 shows T_{rec} only ranging from 3×10^4 to 5×10^4 K for alkalis). Any variation of the chondrule density would affect all elements the same way, and the molecular mass (tens of amu) and condensation coefficients (0.017-0.19 for major lithophile elements; Fedkin et al. (2006)) should be also of the same orders of magnitude. We would need to know those condensation coefficients for the specific elements to make more quantitative comparisons. Elements diffusing slower than alkalis may be affected by mass-dependent diffusivities (see Appendix D), hence perhaps the more negative MDF for Ge (whose tetravalence makes it one of the slowest diffusers reviewed by Zhang et al. (2010)).

However, theoretically, these low $|\text{MDF}|$ values hold in the limit of near-equilibration between gas and melt. As the temperature decreases, $t_{\text{rec}} d\ln X_{\text{buf,j}}/dt$

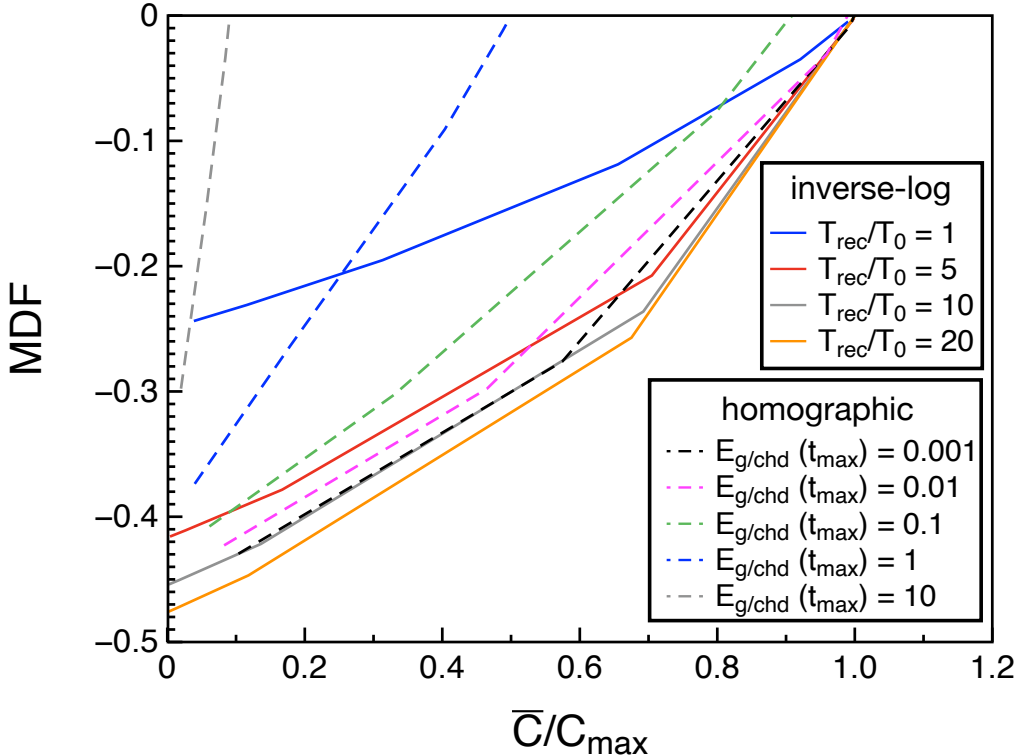


Figure 9: MDF as a function of condensed fraction \bar{C}/C_{\max} for two different cooling laws: a slow cooling interrupted at t_{\max} (*homographic*, dashed line) and an accelerating cooling (*inverse-log*, continuous line). The curves are drawn for different values of parameters ($E_{g/\text{chd}}(t_{\max})$ and T_{rec}/T_0 , respectively, see Appendix C). For low condensed fractions, MDF is usually close to -0.5 unless the condensed fraction was dictated by the quench (at t_{\max} , for the homographic cooling, if $E_{g/\text{chd}}(t_{\max})$ is high).

should become of order unity, and the MDF should be close to -0.5 (according to equation 13), as the chondrule becomes closed to the alkali influx (unless the chondrules have recovered most of them, which is not the case of type I chondrules, dominant in CCs). This is illustrated in Fig. 9 following the calculations of Appendix C for a nonexpanding system. The calculations of Ozawa and Nagahara (2001), assuming constant cooling rates, likewise invariably found final MDF near -0.3. One way out is that the increase of $t_{\text{rec},j}$ suddenly (that is, over a timescale $\ll t_{\text{rec},j}$) accelerated, thus prematurely violating inequation 11 (because of the second derivative of $X_{\text{buf},j} = n_j \pi a^2 \alpha_j (1 - \phi) v_{T,j} t_{\text{rec},j}$). This would cut short any further (near-)equilibration, and the cooling rate in equation 16 would then refer to that before this cooling acceleration. Such a quenching is supported by the preservation of glassy mesostasis (requiring cooling rates in excess of 360-1800 K/h or 1-10 K/h for basaltic and rhyolitic melt compositions, respectively, near plausible glass transition temperatures of 680-880°C; Jones et al. (2018)), the frequent monoclinic structure of low-Ca pyroxene (requiring 250-10000 K/h around 1000°C; e.g. Soulié, 2014), or the low density of dislocations in olivine (suggesting quenching above 1000°C; Jones et al. (2018)). These indeed contrast with evidence for slower cooling rates at higher temperatures for type I chondrules, e.g. from Cu-Ga zoning in metal grains (0.5-50 K/h at $1200 \pm 100^\circ\text{C}$; Humayun (2012); Chaumard et al. (2018)), clinopyroxene exsolution lamellae (0.1-50 K/h at 1200-1400°C; Weinbruch et al. (2001)) or mesostasis-olivine partitioning equilibration of trace elements ($\lesssim 10$ K/h; Jacquet et al. (2012)). So (type I) chondrules do seem to have undergone a quench (e.g. Jacquet et al., 2012; Villeneuve et al., 2015; Libourel et al., 2023), perhaps upon their exit from their hot melting region.

4.3. Alkali-zoned chondrules

How are we to understand alkali-zoned chondrules, with alkalis increasing toward their rims (Matsunami et al., 1993; Grossman et al., 2002; Libourel et al., 2003; Nagahara et al., 2008)? In many cases, Na_2O is positively correlated with SiO_2 (both increasing outward), and thus anticorrelated with optical basicity, as in the general population of chondrules (Fig. 10). Yet, as in the latter, this is a stronger dependence than a uniform $\text{NaO}_{0.5}$ activity throughout the chondrule interior would impose. This is at variance with the conclusion of Appendix D that diffusion transport was efficient when chondrules closed themselves to alkali recondensation. Grossman et al. (2002) also

Table 2: Mass-dependent fractionations for different elements arranged in order of decreasing CI-normalized abundances ("chd/CI") in CC chondrules (generally the extrapolated "non-matrix component", except for Li where individually measured Allende chondrules could be averaged). $\delta^{i/j} E$ is expressed in $\text{\textperthousand} \equiv 10^{-3}$, with 2σ errors given. The MDF are calculated assuming a CI isotopic composition of the pre-chondrule formation reservoir.

E	chd/CI	i	j	$\delta^{i/j} E_{\text{CI}} (\text{\textperthousand})$	$\delta^{i/j} E_{\text{chd}} (\text{\textperthousand})$	MDF	Reference
Li	0.29	7	6	3.6 ± 0.7	-0.3 ± 0.8	-0.02 ± 0.01	Seitz et al. (2007, 2012)
K	0.48	41	39	-0.07 ± 0.03	-0.33 ± 0.12	-0.005 ± 0.002	Nie et al. (2021)
Rb	0.43	87	85	0.17 ± 0.02	0.04 ± 0.05	-0.006 ± 0.002	Nie et al. (2021)
Ge	0.25	74	70	1.00 ± 0.04	$-2.62^{+0.87}_{-1.13}$	-0.06 ± 0.02	Wölfer et al. (2025)
Te	0.15	130	125	0.86 ± 0.19	-0.47 ± 0.30	-0.03 ± 0.01	Morton et al. (2024)
Zn	0.11	66	64	0.45 ± 0.10	-0.10 ± 0.03	-0.018 ± 0.003	Morton et al. (2024)
Cd	0.11	114	110	0.38 ± 0.17	-0.19 ± 0.27	-0.02 ± 0.01	Morton et al. (2024)

argued against diffusion because of the near parallel profiles for elements with different diffusivities.

These objections assume that the chondrules were always single, isolated entities (apart from gas-melt exchange). However, Jacquet (2021) made the case that most chondrules have undergone collisions while partially molten, producing visible compound chondrules when the relaxation to sphericity was longer than cooling. The coarse-grained (igneous) rims around many chondrules were ascribed to the aggregation of smaller droplets (e.g. microchondrules) around bigger objects near the end of cooling (rather than the secondary melting of dust mantles accreted after solidification; Jacquet (2021)). Since those smaller droplets would have equilibrated with the gas at lower temperatures (all else being equal), or have arisen by collisional disruption preferentially in denser areas, they would tend to be SiO_2 - and alkali-enriched.

There would have been a temperature below which diffusion would not have been able to homogenize the chondrules. It would be comparable to the temperature at which compound chondrules made of subequal components can no longer relax to sphericity (after the quench), 1220-1360 K in the estimates of Jacquet (2021) (much lower than typical liquidus temperatures, e.g. 1500-2200 K according to Hewins and Radomsky (1990)). Indeed, by taking into account the effect of crystals on diffusivity and the π^2 factor in the definition of the diffusion timescale t_{diff} (Appendix D), the ratio of the latter to the sphericization timescale t_{sph} is corrected from equation 5 of Jacquet

(2021) as:

$$\begin{aligned}\frac{t_{\text{diff}}}{t_{\text{sph}}} &= \frac{a\gamma(1-\phi)^{3/2}(1+\phi/w)}{\Omega_E T \pi^2} \\ &= 4 \left(\frac{a}{0.3 \text{ mm}} \right) \left(\frac{1-\phi}{0.1} \right)^{3/2} (1+\phi/w) \left(\frac{1000 \text{ K}}{T} \right) \left(\frac{10^{-10} \text{ N/K}}{\Omega_E} \right)\end{aligned}\quad (17)$$

with $\gamma = 0.36 \text{ N/m}$ the surface tension of the melt, ϕ the crystal volume fraction, w a parameter defined in Appendix D and Ω_E the "diffusion factor" of Mungall (2002) for the element E of interest. The latter's normalization value is a suitable upper bound for Na in basalt and andesite (Mungall, 2002). If Na (activity) cannot be homogenized in the melt, the other elements cannot either, and thus their zonings will all essentially follow the boundary between the accreted components, hence the parallelism observed by Grossman et al. (2002). Grossman et al. (2002) themselves entertained late addition of material for some zoned chondrules.

This collisional scenario also accounts for the rarer cases where Na zoning seems decorrelated from optical basicity (Fig. 10). Indeed, droplet composition would not simply be a function of size, but also of precursor nonvolatile element abundances. If the biggest component droplet was e.g. less refractory than average, its melt may have a relatively low optical basicity comparable to that of smaller droplets accreted around it. This would thwart the usual outward decreasing trend of the optical basicity, although alkalis would still increase outward. The diversity of colliding droplets could be further compounded by mixing droplets of different time-temperature histories, e.g. as a function of provenance depth within the chondrule-forming cloud.

5. Consequences on the astrophysical context of chondrule formation

5.1. Chondrule-forming densities

Our scenario of alkali recondensation is depicted in Fig. 11. We have hitherto refrained from commenting on implied densities. With the Alexander et al. (2008) contention that alkali contents were fixed at liquidus set aside, we certainly no longer need values as high as their calculated $0.002 - 9.08 \text{ kg/m}^3$. If we knew what equilibration temperature to substitute, we could

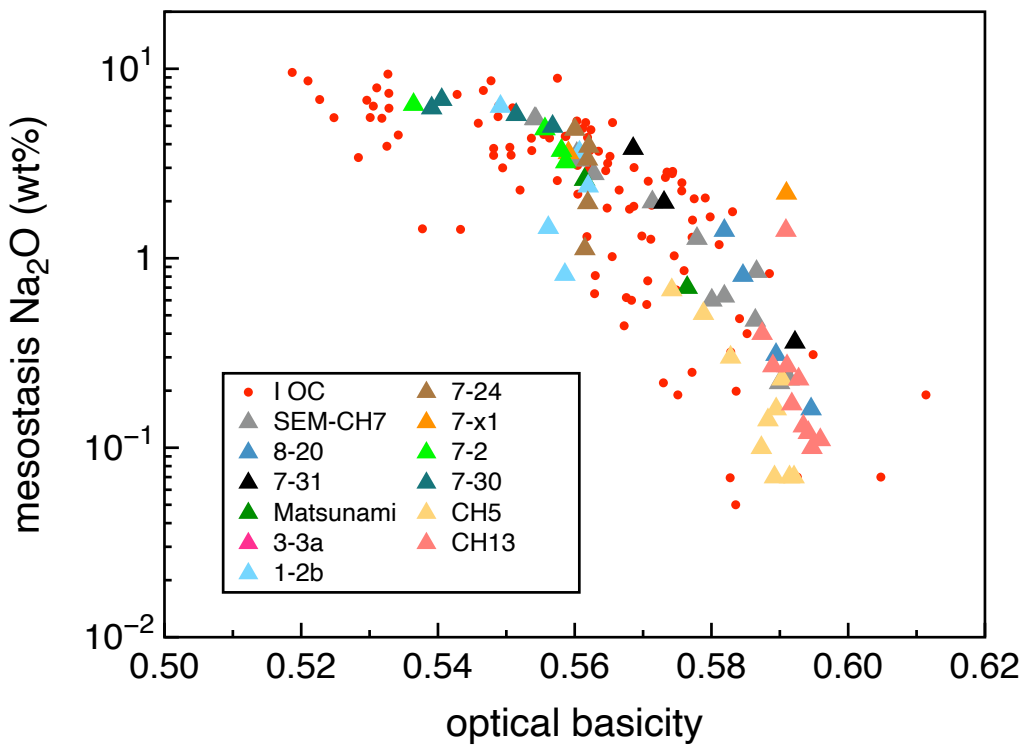


Figure 10: Mesostasis Na₂O versus optical basicity Λ for different alkali-zoned type I chondrules in Semarkona: "Matsunami" (Matsunami et al., 1993), SEM-CH7 (Libourel et al., 2003; Mathieu, 2009), CH5 and CH13 Nagahara et al. (2008) all others from Grossman et al. (2002). They are compared to mesostasis compositions in the general population of type I chondrules in ordinary chondrites.

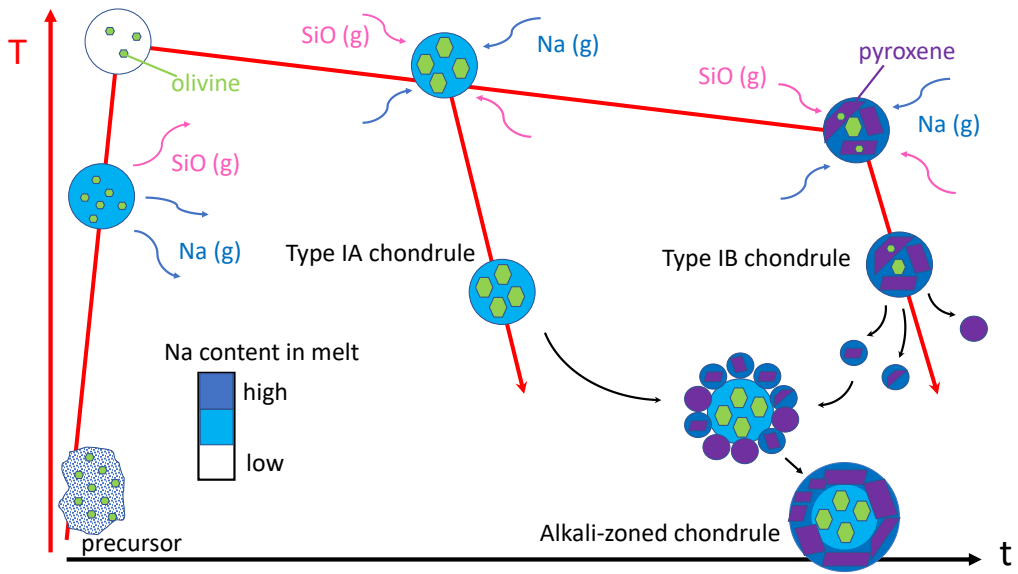


Figure 11: Sketch of our alkali (here, Na) recondensation scenario after the melting and partial evaporation of the precursor (here for type I chondrules). For a given smooth default cooling curve, we show two quench trajectories, one at high temperature leading to a Na-poor type IA (olivine-rich) chondrule, and another at lower temperature leading to a Na-rich type IB (pyroxene-rich) chondrule. Of course all intermediate possibilities (e.g. IAB chondrules) exist. A potential aggregation between high- and low-temperature droplets (here due to disruption of larger chondrules after quenching, but the disruption could have occurred before, or the microdroplets have been small from the outset) leading to an alkali-zoned chondrule is also depicted.

invert equation 4 as:

$$\rho_p = \frac{P_0 K_{\text{Na}} \text{Na}_{\text{chd/g}}}{k_B T f_{O_2}^{1/4} \langle x_l / (\gamma_{\text{NaO}_{0.5}} m_l) \rangle} \quad (18)$$

$$= 1.3 \times 10^{-4} \text{ kg/m}^3 \left(\frac{\text{Na}_{\text{chd/g}}}{0.1} \right) \left(\frac{1 \text{ mol\%}}{\text{Fa}} \right)^{1/2} \left(\frac{40 \text{ amu}^{-1}}{\langle x_l / (\gamma_{\text{NaO}_{0.5}} m_l) \rangle} \right) \left(\frac{1673 \text{ K}}{T} \right) \exp \left(\left(T_{\text{Na}} - \frac{T_{\text{Fa}}}{4} \right) \left(\frac{1}{1673 \text{ K}} - \frac{1}{T} \right) \right) \quad (19)$$

where the fayalite content Fa of the chondrule-hosted olivine enters via the following relationship (Johnson, 1986), in the presence of enstatite⁴:

$$f_{O_2} = 8.7 \times 10^7 \text{ Fa}^2 \exp \left(-\frac{T_{\text{Fa}}}{T} \right) \approx 0.3 \text{ Fa}^2 f_{O_2, \text{IW}} \quad (20)$$

with $T_{\text{Fa}} = 66623 \text{ K}$, and $\text{Na}_{\text{chd/g}} = f_{\text{Na}} / (1 - f_{\text{Na}})$ may be approximated by equating f_{Na} with the average Al-normalized abundance of Na.

In principle, the closure temperature would correspond to a $t_{\text{rec}} = \tau_{\text{eff}} E_{\text{chd/g}}$ reaching some fraction of the timescale of variation of the temperature $\propto (dT/dt)^{-1}$ so that $E_{\text{chd/g}} \propto \rho_p |dT/dt|^{-1}$. Yet this fraction depends on the shape of the cooling curve, which may not be guessed ab initio, especially given the conjectured quenching.

In fact, the most robust constraint is given by the limited isotopic fractionation of alkalis (and other moderately volatile elements). Inverting equation 16, we obtain:

$$\frac{\rho_p}{|dT/dt|} = 10^{-6} \text{ kg.m}^{-3} \cdot \text{K}^{-1} \cdot \text{h} \left(\frac{-0.005}{\text{MDF}} \right) \left(\frac{f_j (1 - f_j)}{0.2} \right) \left(\frac{\langle \rho_s a \rangle}{1 \text{ kg/m}^2} \right) \left(\frac{0.1}{\alpha_j} \right) \left(\frac{m_j}{39 \text{ amu}} \right)^{1/2} \left(\frac{1500 \text{ K}}{T} \right)^{5/2} \left(\frac{T_{\text{rec}}}{3 \times 10^4 \text{ K}} \right) (1 - \phi)^{-1} \left(1 + \frac{T}{T_{\text{rec}}} \frac{d}{d \ln T} \ln \left(\rho_p x_l (f_{O_2} / f_{O_2, \text{IW}})^{1/4} / m_l \right) + \frac{1}{T_{\text{rec}}} \frac{d}{d \ln T} (T \ln \gamma_{EO_{0.5}}) \right) \quad (21)$$

The explicit temperature dependence does not produce more than a factor of two uncertainty, the f_{O_2} dependence has largely disappeared, though

⁴This thus fails for IIA chondrules in CCs.

the most important effect is incorporated in the T_{rec} , where the exact modelling of the activity coefficient is likewise of subordinate importance. The best constraint would be from potassium, as it should be indeed free from diffusion effect in melt (Appendix D) or in crystals (because of its incompatibility, unlike Li) and the normalizations above are adapted to it. Indeed, type I CMO chondrule mesostases in our compilation have an average CI-normalized K/Al ratio (essentially our f_j , since the mesostasis ratio is the bulk ratio) of 0.19 (± 0.03 , $n=75$). If the cooling rate is assumed to be no smaller than the lowest literature estimates discussed previously ($\sim 0.1\text{K/h}$; Jones et al. (2018)), this indicates $\rho_p \gtrsim 10^{-7} \text{ kg/m}^3$.

Interestingly, the Rb/K ratios of the alkali-poorest chondrules in Allende are up to twice the chondritic value (Matsuda et al., 1990). This suggests that $(\text{Rb/K})_{\text{chd/g}}$ was ~ 2 , which from Appendix B would indicate a quenching temperature around 1250 K. So if this, after all, is a suitable estimate, equation 18 would yield $\rho_p = 6 \times 10^{-6} \text{ kg/m}^3$ (for $\gamma_{\text{Na}_{0.5}}(1673 \text{ K}) = 10^{-4}$).

At the order-of-magnitude level, this is consistent (or may be brought in consistency, see Appendix E) with constraints from limited Mg isotopic fractionations of chondrules, as well as oxygen fugacity and compound chondrule frequencies as depicted in Fig. 12. Such elevated densities are needed to stabilize liquids (Cuzzi and Alexander, 2006). Ebel and Grossman (2000) quote minimum solid/gas enrichments of 12.5 and 425 at 10^{-3} and 10^{-6} bar; corresponding to $\rho_p \approx 10^{-6} \text{ kg/m}^3$ and $4 \times 10^{-8} \text{ kg/m}^3$ (after condensation of all rock-forming elements), respectively.

Yet, astrophysically speaking, this represents a huge value, comparable to the *gas* density at 1 AU for a Minimum Mass Solar Nebula (Hayashi, 1981), although the solar solid/gas (mass) ratio is 10^{-2} (Fig. 12). Solid/gas ratios of order unity, as suggested by fayalite contents in type I (and a fortiori type II) chondrules (e.g. Tenner et al., 2015), would require efficient settling to the midplane, and could be conducive to streaming instabilities. This could be assisted by radial concentration in pressure bumps (e.g. Jacquet et al., 2024). So nebular chondrule-forming scenarios remain viable. At any rate, chondrule-forming densities may not be reached beyond a few AU (Fig. 12), in line with the rarity of chondrules in CI chondrites and C asteroids (e.g. Morin et al., 2022; Nakamura et al., 2023; Lauretta et al., 2024).

5.2. NC/C comparison

The previous subsection has addressed data from carbonaceous chondrites. However, chondrules in the NC superclan seem largely autochthonous

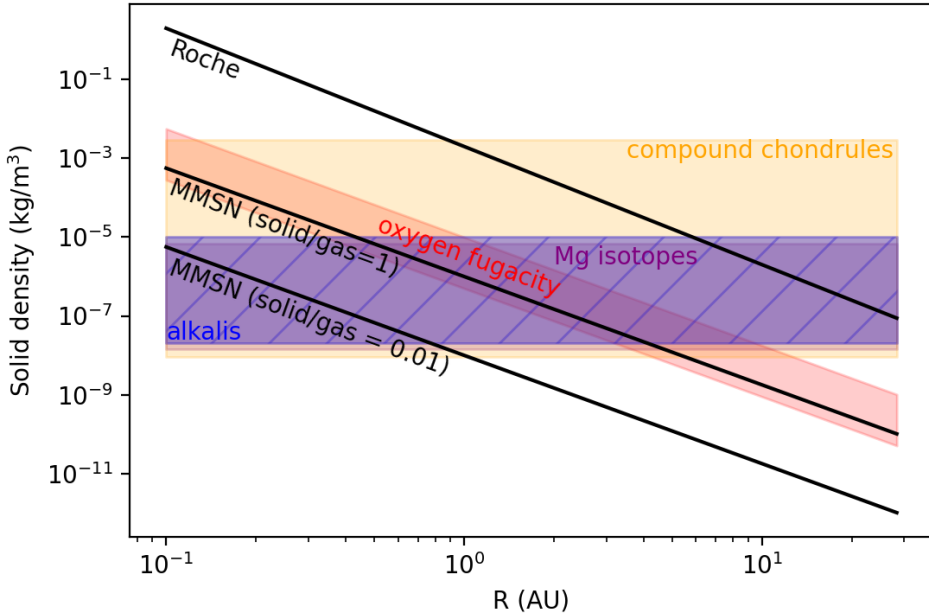


Figure 12: Various constraints from this work and the literature (mutatis mutandis) on chondrule-forming solid densities, as a function of heliocentric distance R , modified after Jacquet et al. (2024), assuming $a = 0.3$ mm. The alkali constraint is derived from this work, chiefly the K isotopic fractionation, assuming no expansion and a (pre-quench) cooling rate comprised between 0.1 and 50 K/h (see discussion in 4.2). The nearly identical Mg isotopic constraint is from Cuzzi and Alexander (2006), with their heating time 2×10^4 s taken as a minimum, and the upper bound differing by the same factor as for the cooling rates selected above for the alkalis. The compound chondrule frequency constraint is taken from Jacquet (2021), with a (post-quench) collision time of 1 h, N_{coag} comprised between 0.1 and 1, and a relative velocity between 0.03 m/s (the bouncing barrier estimate, in pre-chondrule forming nebular conditions (Jacquet, 2014)) and 1 km/s (for droplet integrity; Arakawa and Nakamoto (2019)). The oxygen fugacity constraints are taken from Tenner et al. (2015), which strictly constrain the solid/gas ratio, and thus depends on an assumed gas density, here the midplane Minimum Mass Solar Nebula (MMSN), only for reference (of course this profile does not lead to the pressure bumps advocated in the text). The MMSN midplane dust density is also plotted, as well as a dust-enriched version with dust/gas (mass) ratio of unity conducive to streaming instability, and the Roche density threshold conducive to gravitational collapse.

Table 3: Averaged alkali abundances of type I chondrules. The data are CI-normalized (Lodders, 2003) and based on the averaged composition of chondrule mesostases in our compilation (number n of analyses specified) and errors are one standard error of the mean. The CR average does not include the 50 Mathieu (2009) measurements which seem to have preferentially targeted a few alkali-rich objects.

Group	Na/Al	K/Al	n
EH	1.0 \pm 0.1	1.1 \pm 0.2	56
OC	0.30 \pm 0.02	0.23 \pm 0.02	171
CMO	0.19 \pm 0.02	0.19 \pm 0.02	75
CR	0.13 \pm 0.02	0.26 \pm 0.09	58
CHB	0.16 \pm 0.02	0.09 \pm 0.02	39

to it, judging from their nucleosynthetic isotopic anomalies (e.g. Schneider et al., 2020), and thus formed in a reservoir distinct from the former. How do their alkali elemental and isotopic systematics compare?

In terms of elemental abundances, the NC chondrules have on average higher alkali abundances than their C counterparts, more or less reflected by the bulk chondrite abundances. The difference narrows though if we restrict attention to type I chondrules (that is, similar oxygen fugacities relative to IW), as in table 3. While EH (type I) chondrules show near chondritic alkali abundances, OC are only a factor of \sim 1-3 above their CC counterparts. OC, CMO and CR chondrules show overlapping alkali vs. SiO_2 trends after averaging (Fig. 6, 7).

In terms of isotopic composition, OC chondrules measured by Koefoed and Wang (2025) average $\delta^{41/39}\text{K}=-1\text{\textperthousand}$, which, if tied to the same (CI) chondrule-forming reservoir composition, would yield an MDF three times that of carbonaceous chondrites. Since enstatite chondrites exhibit bulk potassium isotopic ratios intermediate between bulk ordinary chondrites and extrapolated CC chondrules, the MDF of their chondrules should be intermediate as well. Likewise, Wang et al. (2025) measured an average $\delta^{87/85}\text{Rb}=0.12\pm0.02\text{\textperthousand}$ for EH3 chondrites, which, if identified with the chondrule composition, would yield an MDF double that of CC chondrules. Semarkona chondrules yield an average $\delta^{7/6}\text{Li}=0.4\text{\textperthousand}$ not much heavier than Allende chondrules (Seitz et al., 2012).

Given the orders of magnitude over which ρ_p might be expected to vary between the inner and the outer disk (in an MMSN, for example, it scales like $R^{-2.75}$ with R the heliocentric distance; see Fig. 12), it is surprising the ele-

mental abundances and estimated MDF (both dependent on $\rho_p/|dT/dt|$) only differ by a factor of a few. "Planetary" scenarios where chondrule-forming conditions (e.g. an impact plume) are decoupled from the surrounding disk could find comfort in such evidence (even though that from precursor composition would remain problematic; Marrocchi et al. (2024)). There is however some evidence that cooling was slower for the CC chondrules. Most chondrule mesostases in CV (Brearley and Jones, 1998) and CR (Harju et al., 2014) chondrites are holocrystalline, not glassy, and about 10 % of chondrules in CO chondrites are plagioclase-bearing, which the Wick and Jones (2012) experiments only reproduced for their slowest cooling rate of 1 K/h. The suprachondritic Rb/K ratios reported in the alkali-poorest Allende chondrules discussed previously are not seen in ordinary chondrites, with chondritic (Alexander, 1994) or subchondritic (Grossman et al., 2007) values being measured in LL3 chondrites, so this would suggest higher equilibration temperatures. To achieve similar $\rho_p/|dT/dt|$ ratios, faster cooling rates for NC chondrules would mean higher chondrule-forming densities, in line with their shorter heliocentric distances of formation. We note that $\delta^{41/39}\text{K}$ (and thus MDF) does not seem to change between type I and (faster cooled; Jacquet et al. (2015b)) type II chondrules in OCs (Koefoed and Wang, 2025), so this approximate compensation between chondrule-forming densities and cooling rates also applied within single chondrule-forming reservoirs.

Why would there be such a compensation? Perhaps the cooling rate was dictated by the exit from the hot chondrule-forming region, whose "boundary" may have had an optical depth of order unity. Since the opacity would have been proportional to ρ_p , for a given relative velocity, the timescale of the exit would have been inversely proportional to it, and thus the cooling rate would have been proportional to ρ_p . This is only speculative at this point; this compensation would remain a constraint on specific chondrule-forming processes (Jacquet et al., 2015b).

5.3. Perspectives

In this contribution, we have offered a synthesis on the incorporation of alkali elements in chondrules, undertaking to account for bulk composition, mesostasis and glass inclusions, olivine zoning, isotopic compositions and the alkali-zoned chondrules. However, this work is not a full modelling of the evolution of chondrules in a gas. It is rather a collection of theorems based on broad assumptions, independent of details of such a modelling (e.g. specific

cooling curves), and expressed as a function of parameters (e.g. condensation coefficients, crystal fraction etc.) which are not explicitly modelled (and could vary with time), though constrained in order of magnitude. Certainly, real *ab initio* kinetic calculations on the evolution of melt compositions in interaction with the gas in dust-enriched systems would be desirable (if only to test the validity of the assumptions), first in an homogeneous medium ("0D"), later perhaps introducing some spatial heterogeneities. We also encourage more cooling rate constraints on chondrules from both C and NC superclans, bearing in mind the possibility (advocated here) of nonlinear (and more specifically, accelerating) cooling. More measurements of different alkalis (e.g. the Rb/K ratio) of chondrules in different chondrite groups would be desirable. We also encourage more experiments or theoretical treatment on the condensation coefficients of alkalis and other moderately volatile elements to help model all those simultaneously beyond the order-of-magnitude level which we have had to be content with.

Acknowledgments

This work was supported by ANR PERSEID (ANR-25-CE49-3880). We thank Alessandro Morbidelli and Roger Hewins for discussions. The paper is dedicated to the memory of the first author's great-aunt Claire Passe and great-uncle Jean Passe.

Appendix A. Calculation of activity coefficients

The activity of $\text{NaO}_{0.5}$ in the melt may be written as:

$$a_{\text{NaO}_{0.5}} = \sqrt{a_{\text{Na}_2\text{O}}} \equiv \gamma_{\text{NaO}_{0.5}} x_{\text{NaO}_{0.5}} \quad (\text{A.1})$$

with $\gamma_{\text{NaO}_{0.5}}$ the activity coefficient and

$$x_{\text{NaO}_{0.5}} = \frac{m_l}{m_{\text{Na}}} \text{Na}_l \quad (\text{A.2})$$

the molar fraction, expressed here as a function of the mass fraction in the liquid Na_l and the mean "molecular" mass m_l . So as to fit with Mathieu (2009); Mathieu et al. (2011), except for the trace alkalis (as only the single-cation "molecules" satisfy Henry's law), the "molecules" in question are: $\text{NaO}_{0.5}$, $\text{KO}_{0.5}$, MgO , Al_2O_3 , SiO_2 , P_2O_5 , CaO , TiO_2 , Cr_2O_3 , MnO , FeO . So

Table A.4: Optical basicity

oxide	MgO	Al ₂ O ₃	SiO ₂	P ₂ O ₅	CaO	TiO ₂	MnO	FeO
Λ	0.78	0.6	0.48	0.4	1	0.61	1	1

Table A.5: Activity coefficient for NaO_{0.5} at 1400 °C

Λ	0.48	0.55	0.60	0.65	0.72
$\gamma_{\text{NaO}_{0.5}}$	3.8×10^{-5}	8×10^{-5}	1.5×10^{-4}	2×10^{-3}	2×10^{-2}

in this convention, m_l is of order 60 g/mol (roughly the molecular mass of SiO₂).

Judging from the Na₂O (mol%) vs. P_{Na} diagram (Fig. V.18) of Mathieu (2009), chondrule mesostasis compositions should be in the Henry domain. The applicable $\gamma_{\text{NaO}_{0.5}}$ would then be calculable from the initial slopes a_{Mathieu} in this diagram, using the action mass law, as⁵:

$$\gamma_{\text{NaO}_{0.5}} = \frac{f_{O_2}^{1/4}}{2K_{\text{Na}}a_{\text{Mathieu}}P_0} \quad (\text{A.3})$$

From table V.5 of Mathieu (2009) for experiments at 1400 °C (and the NNO buffer at $f_{O_2} = 2.11 \times 10^{-6}$), we calculate the values tabulated in Table A.5. These are a function of the (volatile-free) optical basicity, which is the average (weighted by oxygen atoms) of the pure oxide values tabulated in table A.4 below (Mathieu, 2009):

Mesostasis values have then been estimated using a Lagrange polynomial interpolation of the logarithms of its values at $\Lambda=0.48$, 0.55 and 0.60. For (more optically basic) bulk silicate chondrules, the interpolation was for $\Lambda=0.55$, 0.60 and 0.65.

These are activity coefficients for a specific temperature (1673 K). For a regular solution, $\ln\gamma \propto T^{-1}$ (e.g. Ghiorso and Sack, 1995). This is essentially the behavior shown in fits for $T \ll 10^4$ K (Zhang et al., 2021; Wolf et al., 2023). So we will adopt:

$$\gamma_{\text{NaO}_{0.5}}(\chi, T) = \gamma_{\text{NaO}_{0.5}}(\chi, 1673\text{K})^{\frac{1673\text{K}}{T}} \quad (\text{A.4})$$

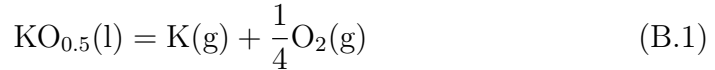
⁵In the limit of vanishing sodium contents, the molar fraction of Na₂O (all other above molecular species equal) is $x_{\text{NaO}_{0.5}}/2$

with χ symbolizing the chemical composition of the melt, and the same for the other alkalis.

Appendix B. Thermodynamics of recondensation of other alkalis

Appendix B.1. Potassium

The reaction constant of



is :

$$K_K = 8.7 \times 10^5 \exp\left(-\frac{26207\text{K}}{T}\right) \quad (\text{B.2})$$

At large densities, some of the vapor phase K may be in the form of KCl (Ebel and Grossman, 2000). However, this cannot be a majority above the half-condensation temperatures of the alkalis. Indeed, if we let

$$K_1 = 1.4 \exp\left(\frac{1822\text{K}}{T}\right) \quad (\text{B.3})$$

the constant (fitted for T between 1200 and 3000 K) of the reaction



we find:

$$\frac{n_{\text{KCl}}}{n_K} = K_1 \frac{n_{\text{NaCl}}}{n_{\text{Na}}} \lesssim K_1 \left(\frac{\text{Cl}}{\text{Na}}\right)_g = 0.13 \frac{(\text{Cl/Na})_g}{(\text{Cl/Na})_{\text{CI}}} \exp\left(\frac{1822\text{K}}{T}\right) \quad (\text{B.5})$$

where $(\text{Cl/Na})_{g,\text{CI}}$ are the atomic Cl/Na ratio in the gas phase and CI chondrites, respectively. This is thus $\ll 1$ so long Na has not significantly recondensed. Part of the gas phase Cl would also be locked in HCl so this is a conservative upper bound. So we might not expect more than a factor of two decrease of the K/Na ratio in the monoatomic gas relative to elemental abundances.

Assuming both Na and K are equilibrated with the gas, the ratio of the K/Na ratios in the liquid and in the monoatomic gas is:

$$(\text{K/Na})_{\text{chd/g}} = \frac{\gamma_{\text{NaO}_{0.5}}}{\gamma_{\text{KO}_{0.5}}} \frac{K_{\text{Na}}}{K_K} = 1.1 \exp\left(\left(1673 \ln \frac{\gamma_{\text{NaO}_{0.5}}(1673\text{K})}{\gamma_{\text{KO}_{0.5}}(1673\text{K})} - 4479\right) \frac{\text{K}}{\text{T}}\right) \quad (\text{B.6})$$

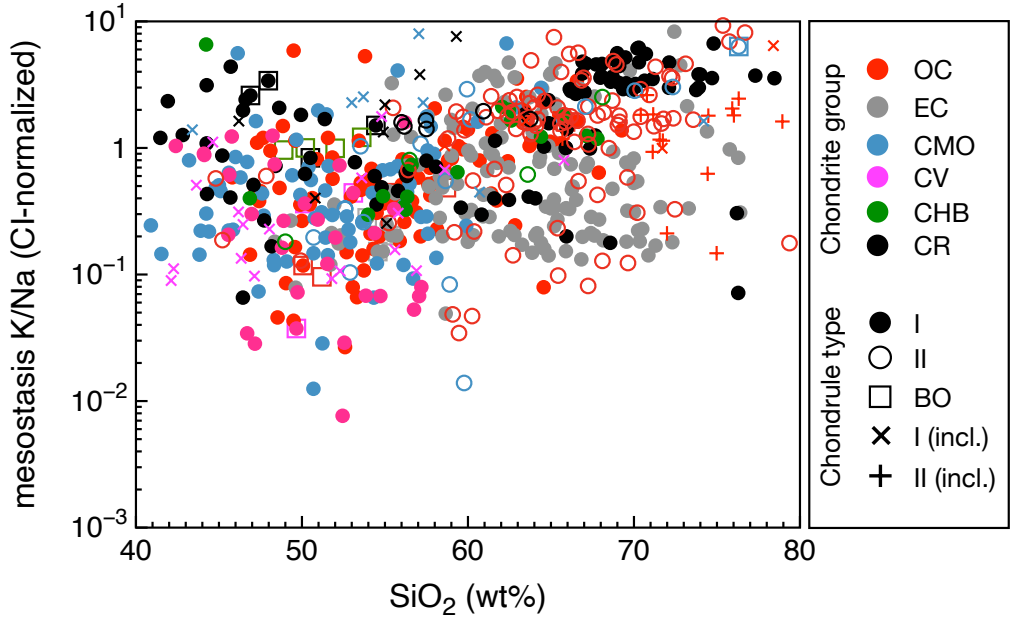


Figure B.13: Mesostasis K/Na ratio vs. silica.

We have no activity coefficient model for $\text{KO}_{0.5}$, as the Georges (2000) parameterization of the solubility of K is only applicable for much more Ca-rich (30–45 wt% CaO) and Al-poor compositions than chondrule mesostases, and the MELTS code yields spurious results (Zhang et al., 2021). For a basaltic composition, the values reported by Zhang et al. (2021) yield $\gamma_{\text{NaO}_{0.5}}/\gamma_{\text{KO}_{0.5}} = 24$ (for identical evaporation coefficients) so $(\text{K}/\text{Na})_{\text{chd/g}} = 1.8$ at 1673 K.

However, mesostasis data suggest that the most basic melts show sub-chondritic K/Na ratios (Fig. B.13). This includes olivine-hosted glass inclusions and barred olivine (BO) chondrule mesostases which were presumably instantly sealed off further interaction with the gas (by shell formation upon nucleation for BO chondrules). This may come about because half of gaseous K was locked in KCl as mentioned above, or uncertainties in the thermodynamic data. More silica-rich melts may have higher $\gamma_{\text{NaO}_{0.5}}/\gamma_{\text{KO}_{0.5}}$ hence higher K/Na ratios, which could also come about by the increase of the K/Na ratio of the residual gas in K if $(\text{K}/\text{Na})_{\text{chd/g}}$ was actually below unity.

Appendix B.2. Rubidium

We may likewise express the reaction constant (Sossi et al., 2019)

$$K_{\text{Rb}} = 2.1 \times 10^{13} \exp\left(-\frac{48400 \text{ K}}{T}\right) \quad (\text{B.7})$$

Thus:

$$(\text{Rb}/\text{K})_{\text{chd/g}} = \frac{\gamma_{\text{KO}_{0.5}}}{\gamma_{\text{RbO}_{0.5}}} \frac{K_{\text{K}}}{K_{\text{Rb}}} = \exp\left(22193 \text{ K} \left(\frac{1}{T} - \frac{1}{1300 \text{ K}}\right)\right) \frac{\gamma_{\text{KO}_{0.5}}}{\gamma_{\text{RbO}_{0.5}}} \quad (\text{B.8})$$

The Zhang et al. (2021) experiments suggest that $\gamma_{\text{KO}_{0.5}} = \gamma_{\text{RbO}_{0.5}}$. So $(\text{Rb}/\text{K})_{\text{chd/g}}$ increases with decreasing temperature and becomes unity at 1300 K.

Appendix B.3. Lithium

Likewise, from Sossi et al. (2019):

$$K_{\text{Li}} = 1.8 \times 10^7 \exp\left(-\frac{49673 \text{ K}}{T}\right) \quad (\text{B.9})$$

Thus

$$(\text{Li}/\text{Rb})_{\text{chd/g}} = \frac{\gamma_{\text{KO}_{0.5}}}{\gamma_{\text{LiO}_{0.5}}} \frac{K_{\text{Rb}}}{K_{\text{Li}}} = 2 \times 10^6 \frac{\gamma_{\text{RbO}_{0.5}}}{\gamma_{\text{LiO}_{0.5}}} \exp\left(1273 \text{ K} \left(\frac{1}{T} - \frac{1}{1673 \text{ K}}\right)\right) \quad (\text{B.10})$$

Sossi et al. (2019) report $\gamma_{\text{LiO}_{0.5}} = 1.8 \pm 0.2$ and $\gamma_{\text{RbO}_{0.5}} = (1.3 \pm 0.15) \times 10^{-4}$ in a ferrobasaltic melt at IW-8 and 1400 °C, so this should be 180 then. Li is thus more refractory than the other alkalis.

Table B.6 summarises the Arrhenian temperature dependences of the alkalis.

Appendix C. Mass-dependent fractionation in a closed chondrule-forming volume

We consider a homogeneous volume containing gas and a population of identical chondrules, with N_i the total number density of isotopes i . Then, expressing $n_i = N_i - n_p X_i$, with n_p the number density of chondrules, the Hertz-Knudsen equation 8 may be rewritten as:

$$\frac{dX_i}{dt} = \frac{X_{\text{conv},i} - X_i}{t_{\text{conv},i}} \quad (\text{C.1})$$

Table B.6: Arrhenian temperature dependences. The T_{rec} are calculated for the indicated, typical values of $\gamma_{\text{EO}_{0.5}}(1673 \text{ K})$.

E	T_E (K)	$\gamma_{\text{EO}_{0.5}}(1673 \text{ K})$	$T_{\text{rec},E}$ (K)
Li	49673	1	33108
Na	30686	10^{-4}	29619
K	26207	10^{-5}	28903
Rb	48400	10^{-5}	51096

where

$$t_{\text{conv},i} = \left(\frac{1}{t_{\text{rec},i}} + \frac{1}{\tau_{\text{eff},i}} \right)^{-1} \quad (\text{C.2})$$

$$X_{\text{conv},i} = \frac{N_i/n_p}{1 + \tau_{\text{eff},i}/t_{\text{rec},i}} \quad (\text{C.3})$$

The formal solution of equation C.1, evaluated at the end of the cooling ($t = t_{\text{max}}$) is:

$$\begin{aligned} X_i &= \int_0^{t_{\text{max}}} \frac{de^{-x_i}}{dt} X_{\text{conv},i} dt + X_i(0) \exp \left(- \int_0^{t_{\text{max}}} \frac{dt}{t_{\text{conv},i}} \right) \\ &\approx \int_0^{t_{\text{max}}} \frac{de^{-x_i}}{dt} X_{\text{conv},i} dt \end{aligned} \quad (\text{C.4})$$

with the "memory variable"

$$x_i \equiv \int_t^{t_{\text{max}}} \frac{dt'}{t_{\text{conv},i}} \quad (\text{C.5})$$

and where the approximation assumes the limit of forgotten beginnings (i.e. $x_j(0) \gg 1$). Of course, the same equations obtain for isotope j . We now assume no equilibrium isotopic fractionation, that is $X_{\text{conv},i}/X_{\text{conv},j} = N_i/N_j$ (as reported for K by Nie et al. (2021)). Since $x_i = x_j \sqrt{m_j/m_i}$, we have:

$$\frac{X_i/X_j}{N_i/N_j} - 1 \approx \left(1 - \sqrt{\frac{m_j}{m_i}} \right) \frac{1}{X_j} \int_0^{t_{\text{max}}} \frac{d}{dt} (x_j e^{-x_j}) X_{\text{conv},j} dt \quad (\text{C.6})$$

Thus:

$$\text{MDF} \approx \frac{1}{2} \left(-1 + \frac{1}{X_j} \int_0^{t_{\text{max}}} x_j e^{-x_j} \frac{X_{\text{conv},j}}{t_{\text{conv},j}} dt \right) \quad (\text{C.7})$$

We now assume that both $X_{\max,j} \equiv N_j/n_p$ and $\tau_{\text{eff},j} = (n_p \pi a^2 \alpha_j v_{T,j} (1 - \phi))^{-1}$ were constant, which, given that $a^2 T^{1/2} \alpha_j (1 - \phi)$ likely only weakly varied during recondensation, essentially amounts to constant n_p and N_j (i.e. no volume change of the gas+chondrules parcel). Since $X_{\text{conv},j}/t_{\text{conv},j} = X_{\max,j}/\tau_{\text{eff},j}$ would have been likewise constant, we have:

$$X_j = X_{\max,j} \int_0^{t_{\max}/\tau_{\text{eff},j}} e^{-x_j} dz \approx X_{\max,j} \int_0^{\infty} e^{-x_j} dz \quad (\text{C.8})$$

where we have introduced the normalized look-back time $z = (t_{\max} - t)/\tau_{\text{eff},j}$ and pushed the limit of the integral over that variable to infinity (for any integrable monotonic extrapolation of the integrand before time zero) owing to the assumed limit of forgotten beginnings (effectively removing $t_{\max}/\tau_{\text{eff},j}$ as a parameter). Likewise:

$$\text{MDF} = \frac{1}{2} \left(-1 + \int_0^{\infty} x_j e^{-x_j} dz / \int_0^{\infty} e^{-x_j} dz \right) \quad (\text{C.9})$$

with

$$x_j = z + \int_t^{t_{\max}} \frac{dt}{t_{\text{rec},j}} \quad (\text{C.10})$$

We will neglect non-Arrhenian dependences in $t_{\text{rec},j} \propto e^{T_{\text{rec}}/T}$. To completely express x_j and entirely determine the calculations above, we need to prescribe the time-temperature (t - T) histories. We will consider two endmember possibilities. The first is the *homographic* cooling

$$T = \frac{T_0}{1 + t/t_0} \quad (\text{C.11})$$

exemplifying a slowing cooling (for $t < t_{\max}$, zero afterward), and the second is the *inverse-log* cooling

$$T = -\frac{T_0}{\ln(1 - t/t_{\max})} \quad (\text{C.12})$$

with an accelerating cooling for $(1 - e^{-2})t_{\max} \leq t < t_{\max}$ ⁶. These functional forms are only motivated by mathematical simplicity, for Arrhenian temperature dependences translate into easily integrable exponential and power law time dependences for the homographic and inverse-log forms, respectively.

⁶The inflection before then will not matter for we will assume that $T_0/2 = T((1 - e^{-2})t_{\max})$ is much higher than the final equilibration temperature so no memory is retained from this part.

Indeed, for the homographic cooling, we obtain:

$$x_j = z + E_{\text{g/chd}}(t_{\max}) (e^{z/z_0} - 1) z_0 \quad (\text{C.13})$$

with $E_{\text{g/chd}}(t_{\max}) = \tau_{\text{eff,j}}/t_{\text{rec,j}}(t_{\max})$ the final equilibrium gas/chondrule budget ratio and

$$z_0 = \frac{T_0 t_0}{T_{\text{rec}} \tau_{\text{eff,j}}} \quad (\text{C.14})$$

For the inverse-log cooling, we have:

$$x_j = z \left(1 + \frac{1}{1 + T_{\text{rec}}/T_0} \left(\frac{z}{z_{50}} \right)^{T_{\text{rec}}/T_0} \right) \quad (\text{C.15})$$

with z_{50} the normalized look-back time corresponding to (equilibrium) half-condensation.

Fig. 9 plots the MDF for different values of $E_{\text{g/chd}}(t_{\max})$ (homographic) and T_{rec}/T_0 (inverse-log). The MDF are generally close to -0.5 especially for low condensed fractions. The homographic cooling only achieves low absolute MDF when the condensed fraction is near the equilibrium one at t_{\max} , i.e. $(1 + E_{\text{g/chd}}(t_{\max}))^{-1}$ and thus effectively imposed by a quench. The inverse-log cooling would take $T_{\text{rec}}/T_0 < 1$ to remotely compete, which would also amount to a quench. Indeed, with T_{rec} being a few $10^4 K$ (Appendix B), the half-condensation temperature T_{50} would be reached in the steep decrease part of the cooling as $T_{50} \ll T_{\text{rec}} < T_0$.

Appendix D. Effect of diffusion

The derivations in section 4 assumes that the chondrule melt is well-mixed. This appendix examines this assumption from the point of view of diffusion in the melt. (One could also envision the possibility of turbulent motions in that melt enhancing transport without any isotopic selectivity).

Appendix D.1. Diffusion timescale

Generally speaking, diffusion coefficients in a melt D follow an Arrhenian dependence of the form:

$$D = D_0 \exp(-T_D/T) = D(1673\text{K}) \exp\left(T_D \left(\frac{1}{1673\text{K}} - \frac{1}{T} \right)\right) \quad (\text{D.1})$$

It is somewhat uncertain what the relevant parameterization for chondrule mesostasis is, as D_0 and T_D (that is, the activation energy divided by the gas constant) depend on melt composition. Yet a "compensation rule" seems to maintain $D(1673 \text{ K})$ around $10^{-9} \text{ m}^2/\text{s}$ for Na (Lowry et al., 1982; Mungall, 2002; Zhang et al., 2010) so most of the uncertainty resides on T_D . For other alkalis, Zhang et al. (2021) report similar 1673 K diffusivities of 1.05×10^{-9} and $1.2 \times 10^{-9} \text{ m}^2/\text{s}$ for Rb and K in a basaltic melt. However, compilations by Zhang et al. (2010); Mungall (2002) indicate lower diffusion coefficients (by 1-2 orders of magnitude) for more silica-rich compositions for those alkalis. In either case T_D takes typical values of $1-2 \times 10^4 \text{ K}$ (e.g. Zhang et al., 2010; Lowry et al., 1982), with basaltic melts on the higher end of the range. As will matter later, these are lower than calculated T_{rec} values (table B.6; Ozawa and Nagahara (2001)).

Since a chondrule is only partially molten, the applicable effective diffusion coefficient is reduced. Neglecting diffusion through the crystals, an empirical relationship may be given by (Crank, 1975):

$$D_{\text{eff}} = \frac{1 - \phi}{1 + \phi/w} D \quad (\text{D.2})$$

with ϕ the volume fraction of crystals and w a dimensionless, shape-dependent parameter (2 for a sphere).

We define the diffusion timescale as:

$$\begin{aligned} t_{\text{diff}} &= \frac{a^2}{\pi^2 D_{\text{eff}}} \\ &= 9 \text{ s} \left(\frac{a}{0.3 \text{ mm}} \right)^2 \left(\frac{1 - \phi}{1 + \phi/w} \right) \left(\frac{10^{-9} \text{ m}^2/\text{s}}{D(1673 \text{ K})} \right) \exp \left(T_D \left(\frac{1}{T} - \frac{1}{1673 \text{ K}} \right) \right) \end{aligned} \quad (\text{D.3})$$

where the π^2 factor naturally arises in the calculation of the next subsection. (From Fig. 6.1 of Crank (1975), for a constant surface concentration with zero initial inner concentration, this is a good estimate for the time for the center to reach half that surface concentration). Since t_{rec} increases more steeply with cooling (as $T_{\text{rec}} > T_D$), the diffusion timescale would be indeed expected to be shorter than it when alkalis condense quantitatively. This was also observed in the evaporation experiments of Tsuchiyama et al. (1981), whose chondrule analogs had uniform (more or less depleted) Na concentrations. Let us now examine more quantitatively the effect of diffusion.

Appendix D.2. Diffusion in a sphere under recondensation

Assuming a partially molten chondrule devoid of alkalis at time $t = 0$, the concentration $C_i(r, t)$ (atoms per unit volume) of an isotope i of the melt/crystal mix may be written in terms of its surface value $C_i(a, t)$, as a function of distance to center $r < a$ and time t , as:

$$C_i(r, t) = 2 \sum_{n=1}^{\infty} (-1)^{n-1} \text{sinc} \left(\frac{n\pi r}{a} \right) \int_0^t \frac{\partial e^{-n^2 x_{D,i}}}{\partial t'} C_i(a, t') dt' \quad (\text{D.4})$$

where the equation 6.23 of Crank (1975) has been adapted to a time-varying (yet spatially uniform) $D_{\text{eff},i}$ with the diffusion-related memory variable

$$x_{D,i} \equiv \int_{t'}^t \frac{dt''}{t_{\text{diff},i}} \quad (\text{D.5})$$

Thus, neglecting any radius change upon recondensation of the alkalis, its volume-weighted average is:

$$\begin{aligned} \bar{C}_i &= \frac{6}{\pi^2} \sum_{n=1}^{\infty} \frac{1}{n^2} \int_0^t \frac{\partial e^{-n^2 x_{D,i}}}{\partial t'} C_i(a, t') dt' \\ &= C_i(a, t) - \frac{6}{\pi^2} \sum_{n=1}^{\infty} \frac{1}{n^2} \int_0^t e^{-n^2 x_{D,i}} \frac{dC_i(a, t')}{dt'} dt' \\ &\approx C_i(a, t) - \frac{\pi^2}{15} t_{\text{diff},i} \frac{dC_i(a, t)}{dt} \end{aligned} \quad (\text{D.6})$$

where we neglect $C_i(a, 0)$ (the limit of forgotten beginnings) and the final equality assumes $\frac{d}{dt} (t_{\text{diff},i} \frac{d}{dt} C_i(a, t)) / \frac{d}{dt} C_i(a, t) \ll 1$. Thus the Hertz-Knudsen equation

$$\frac{d\bar{C}_i}{dt} = \frac{C_{\text{buf},i} - C_i(a, t)}{t_{\text{rec},i}} \quad (\text{D.7})$$

with $C_{\text{buf},i} \equiv 3X_{\text{buf},i}/(4\pi a^3)$, is a closed integro-differential equation in $C_i(a, t)$.

Appendix D.3. Diffusion- vs. recondensation-limited near-equilibrium

From equations D.6 and D.7, in the limit of short $t_{\text{diff,rec}}$, we have:

$$\bar{C}_i \approx C_{\text{buf},i} - \left(t_{\text{rec},i} + \frac{\pi^2}{15} t_{\text{diff},i} \right) \frac{dC_{\text{buf},i}}{dt} \quad (\text{D.8})$$

Thus, if $D_{\text{eff},i} \equiv D_{\text{eff},j} (m_j/m_i)^\zeta$, we have:

$$\frac{X_i}{X_j} = \frac{\bar{C}_i}{\bar{C}_j} \approx \frac{X_{\text{buf},i}}{X_{\text{buf},j}} \left(1 - \left(t_{\text{rec},j} \left(\sqrt{\frac{m_i}{m_j}} - 1 \right) + \frac{\pi^2}{15} t_{\text{diff},j} \left(\left(\frac{m_i}{m_j} \right)^\zeta - 1 \right) \right) \frac{\text{dln}X_{\text{buf},j}}{\text{dt}} \right) \quad (\text{D.9})$$

Neglecting any equilibrium isotopic fractionation, and assuming a reservoir of identical composition chondrules, we thus calculate:

$$\text{MDF} \approx - (1 - f_j) \left(\frac{f_j}{2} \tau_{\text{eff},j} + (1 - f_j) \frac{\pi^2}{15} \zeta t_{\text{diff},j} \right) \frac{\text{dln}E_{\text{chd/g}}}{\text{dt}} \quad (\text{D.10})$$

Zhang et al. (2021) report ζ values of 0.07 and 0.04 for K and Rb (although for Li it may reach 0.2 (Lesher, 2010)). So the effect of finite t_{diff} is only isotopically appreciable if at least one order of magnitude above t_{rec} . Even in that regime, -MDF will provide an upper bound on the value of $0.5f_j(1 - f_j)\tau_{\text{eff},j}\text{dln}E_{\text{chd/g}}/\text{dt} = 0.5(1 - f_j)^2 t_{\text{rec},j} \text{dln}E_{\text{chd/g}}/\text{dt}$ discussed in section 5.1.

So how important was diffusion for chondrules? If we write⁷

$$t_{\text{rec}} = t_{\text{rec}}(1673 \text{ K}) \exp \left(T_{\text{rec}} \left(\frac{1}{T} - \frac{1}{1673 \text{ K}} \right) \right), \quad (\text{D.11})$$

we can eliminate the Arrhenian factor in the diffusion/recondensation timescale ratio as follows:

$$\frac{t_{\text{diff},j}}{t_{\text{rec},j}} = \frac{t_{\text{diff},j}(1673 \text{ K})}{t_{\text{rec},j}(1673 \text{ K})} \exp \left((T_D - T_{\text{rec},j}) \left(\frac{1}{T} - \frac{1}{1673 \text{ K}} \right) \right) \quad (\text{D.12})$$

$$= \frac{t_{\text{diff},j}(1673 \text{ K})}{t_{\text{rec},j}(1673 \text{ K})} \left(\frac{t_{\text{rec},j}(1673 \text{ K})}{t_{\text{rec},j}} \right)^{1 - T_D/T_{\text{rec},j}} \quad (\text{D.13})$$

(The exponent is positive since T_D is smaller than T_{rec} as mentioned in the

⁷This neglects non Arrhenian dependences, as in Appendix C, or rather, makes the " $t_{\text{rec}}(1673 \text{ K})$ " an Arrhenian extrapolation with non-Arrhenian prefactors evaluated at the real temperature.

first subsection). If indeed negligible in the MDF, we have:

$$\begin{aligned} \frac{t_{\text{diff},j}}{t_{\text{rec},j}} &= t_{\text{diff},j}(1673 \text{ K})t_{\text{rec},j}(1673 \text{ K})^{-T_D/T_{\text{rec},j}} \left(\frac{(1-f_j)^2}{2|\text{MDF}|} \frac{d\ln E_{\text{chd/g}}}{dt} \right)^{1-T_D/T_{\text{rec},j}} \quad (\text{D.14}) \\ &= \left[10^{-3} \left(\frac{t_{\text{diff},j}(1673 \text{ K})[t_{\text{diff},j}(1673 \text{ K})/t_{\text{rec},j}(1673 \text{ K})]^{1/(T_{\text{rec},j}/T_D-1)}}{10 \text{ s}} \right) \right. \\ &\quad \left. \left(\frac{0.01}{|\text{MDF}|} \right) (1-f_j)^2 \left(\frac{100 \text{ K}}{|dT/d\ln E_{\text{chd/g}}|} \right) \left(\frac{|dT/dt|}{10 \text{ K/h}} \right) \right]^{1-T_D/T_{\text{rec},j}} \end{aligned}$$

Diffusion is negligible for isotopic effects if $\zeta t_{\text{diff},j}/t_{\text{rec},j} \ll 1$. This holds for elements diffusing as fast as sodium, or within one or two orders of magnitude thereof, as seems to be the case for K and Rb (Zhang et al., 2021) as mentioned previously.

Appendix D.4. Diffusion under perfect surface-gas equilibrium

The above assumes near-equilibrium. Yet we need to know whether a small $|\text{MDF}|$ necessarily means a quench (in near-equilibrium condition) if diffusion is the rate-limiting step, instead of recondensation examined in Appendix C. We now assume perfect surface equilibration with the gas, i.e. that the surface concentration is buffered at C_{buf} . As in Appendix C, we consider a purely Arrhenian dependence of $E_{\text{chd/g}} = t_{\text{rec},j}/\tau_{\text{eff},j} \propto e^{T_{\text{rec}}/T}$ such that:

$$C_{\text{buf},i} = \frac{C_{\text{max},i}}{1 + \exp\left(T_{\text{rec}}\left(\frac{1}{T_{50}} - \frac{1}{T}\right)\right)} \quad (\text{D.15})$$

where we have introduced the 50 % condensation temperature T_{50} . Unlike Appendix C, this treats the ambient gas partial pressures as given, without thus (explicitly) modeling the feedback of incomplete equilibration of the chondrule population on it. Yet the error on isotopic effects will be limited for the small recondensation fractions of interest for alkalis.

Equation D.6 may then be rewritten as:

$$\bar{C}_i = \frac{6}{\pi^2} \int_0^\infty \sum_{n=1}^\infty e^{-n^2 x_{D,i}} C_{\text{buf},i}(x_{D,i}) dx_{D,i} \quad (\text{D.16})$$

As in Appendix C, we will consider the homographic and inverse-log $T - t$ cooling laws. Thus:

$$x_{D,i} = \int_t^{+\infty} \frac{dt}{t_{\text{diff},i}} = \left(\frac{\pi}{a}\right)^2 \frac{dt}{dD_{\text{eff},i}^{-1}} \times \begin{cases} 1 & \text{(homographic)} \\ (1 + T_0/T_D)^{-1} & \text{(inverse - log)} \end{cases} \quad (\text{D.17})$$

In both cases, we may express:

$$C_{\text{buf,i}} = \frac{C_{\text{max,i}}}{1 + (x_{D,i}/x_{50,i})^\beta} \quad (\text{D.18})$$

with $x_{50,i}$ the value of $x_{D,i}$ at $T = T_{50}$ and

$$\beta = \begin{cases} T_{\text{rec}}/T_D & (\text{homographic}) \\ T_{\text{rec}}/(T_D + T_0) & (\text{inverse - log}) \end{cases} \quad (\text{D.19})$$

In terms of isotopic fractionation, since $x_{50,i} = (m_j/m_i)^\zeta x_{50,j}$, we have:

$$\frac{\bar{C}_i C_{\text{max,j}}}{\bar{C}_j C_{\text{max,i}}} - 1 \approx \frac{\text{dln}\bar{C}}{\text{dln}x_{50}} \left(\left(\frac{m_j}{m_i} \right)^\zeta - 1 \right) \quad (\text{D.20})$$

with

$$\frac{\text{dln}\bar{C}}{\text{dln}x_{50}} = \frac{\beta}{x_{50}^\beta} \sum_{n=1}^{\infty} \int_0^{+\infty} \frac{x^\beta e^{-n^2 x} dx}{(1 + (x/x_{50})^\beta)^2} \left(\sum_{n=1}^{\infty} \int_0^{+\infty} \frac{e^{-n^2 x} dx}{1 + (x/x_{50})^\beta} \right)^{-1} \quad (\text{D.21})$$

This vanishes for $x_{50} \gg 1$ (near-quantitative condensation) and converges toward 0.5 for $x_{50} \ll 1$ (limited recondensation)⁸, hence a MDF of $-\zeta/2$ (Fig. D.14). Below half-condensation, very low β would be required to significantly lower $|\text{MDF}|$. These would correspond to high T_0 in an inverse-log T-t law, hence effectively a quench regime.

The observed $|\text{MDF}|$ (table 2) are much smaller than $\zeta/2$ for ζ values of 0.07 and 0.04 for K and Rb (Zhang et al., 2021). So even if diffusion were the rate-limiting step, a quench would still be required.

Appendix E. Comparison with Mg isotopic constraints

Allende bulk chondrule $\delta^{25}\text{Mg}$ anticorrelates with Mg/Al (Galy et al., 2000), suggestive of Rayleigh fractionation upon evaporation, if much more limited than the vacuum prediction. Cuzzi and Alexander (2006) inferred

⁸Change the integration to variable $y = x/x_{50}$, approximate the Riemann sum $\sum_{n=1}^{\infty} e^{-n^2 x_{50} y} \sim \sqrt{\pi/(x_{50} y)}/2$ and perform an integration by part of the numerator by recognizing $d(1 + y^\beta)^{-1}/dy$.

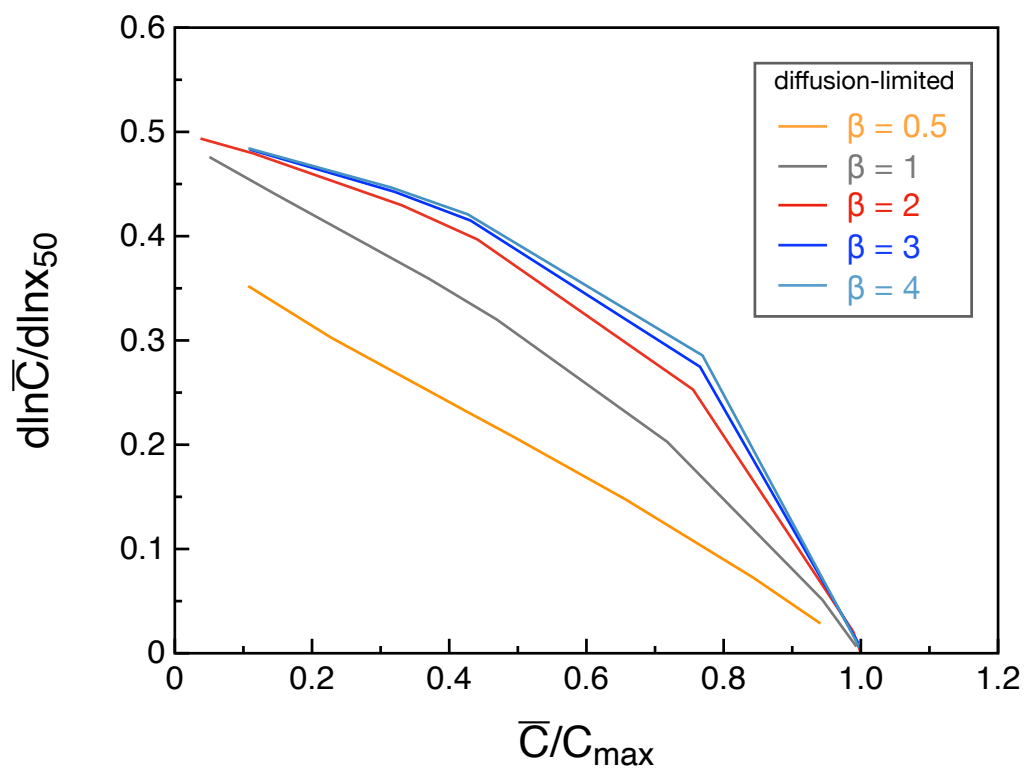


Figure D.14: $d \ln \bar{C} / d \ln x_{50}$ as a function of \bar{C} / C_{\max} .

thence $\rho_p \approx 7 - 13 \times 10^{-6} \text{ kg/m}^3$ to approach Mg saturation sufficiently, consistent with our conclusions, but what they really estimated was the quantity

$$a_{\text{Cuzzi}} \equiv \frac{t_h}{\tau_{\text{eff,Mg}}} \quad (\text{E.1})$$

with t_h the heating time.

Since

$$\text{MDF}_K = -\frac{1}{2} f_K (1 - f_K) \tau_{\text{eff,K}} \frac{d \ln K_{\text{chd/g}}}{dt} \quad (\text{E.2})$$

we have

$$\begin{aligned} \text{MDF}_K a_{\text{Cuzzi}} &= -\frac{1}{2} \frac{\alpha_{\text{Mg}}}{\alpha_K} \sqrt{\frac{m_K}{m_{\text{Mg}}}} f_K (1 - f_K) t_h \frac{d \ln K_{\text{chd/g}}}{dt} (1 - \phi)^{-1} \\ &= -0.13 \left(\frac{\alpha_{\text{Mg}}}{\alpha_K} \right) \frac{f_K (1 - f_K)}{0.2} t_h \frac{d \ln K_{\text{chd/g}}}{dt} (1 - \phi)^{-1} \end{aligned} \quad (\text{E.3})$$

The left-hand-side evaluates to -0.03 from table 2 and the $a_{\text{Cuzzi}} = 6 \pm 1$ obtained by Cuzzi and Alexander (2006). It would require a t_h of order the cooling through one thermal e-fold of K condensation (about 100 K). It seems then difficult to ignore isotopic exchange in the cooling stage. To recover the isotopic fractionations observed, we would need lower densities than calculated by Cuzzi and Alexander (2006) to achieve greater isotopic fractionation before cooling damped them.

The isotopically heavy Mg of the high Al/Mg chondrules of Galy et al. (2000) are however not necessarily related to evaporation *during* chondrule formation. In fact, their Al/Mg ratio may not be either. Indeed, Gerber et al. (2017) found that refractory elements of CV and CR chondrules correlated with their Ti isotopic anomalies, approaching those of CAIs in proportion, and Al-rich chondrules often show REE patterns reminiscent of diluted CAIs (Misawa and Nakamura, 1988; Jacquet and Marrocchi, 2017; Zhang et al., 2020). If the two most Al-rich chondrules (ARC) of Galy et al. (2000), now at an average $\delta^{25}\text{Mg} = 2.55\text{\textperthousand}$, inherited a $\delta^{25}\text{Mg}$ around 10 ‰ from CAI-rich precursors and then exchanged with the gas to approach a buffer value around the Allende bulk value of 1.59 ‰ with an e-folding timescale $\sim t_{\text{rec,Mg}}$ (see equation 12), this would have required an exchange time $t_{\text{exch,Mg}}$ given by:

$$a_{\text{new}} \equiv \frac{t_{\text{exch,Mg}}}{t_{\text{rec,Mg}}} = \ln \left(\frac{10 - 1.59}{2.55 - 1.59} \right) = 2 \quad (\text{E.4})$$

This is only an order-of-magnitude estimate, ignoring variations of $t_{\text{rec,Mg}}$ (which otherwise would have to be replaced by its harmonic time average). And thus:

$$\begin{aligned} \text{MDF}_K a_{\text{new}} &= -\frac{f_{\text{evap,Mg}}}{2} \frac{\overline{\text{Mg}}_{\text{max}}}{\text{Mg}_{\text{ARC}}} \frac{\alpha_{\text{Mg}}}{\alpha_K} \sqrt{\frac{m_K}{m_{\text{Mg}}}} f_K (1 - f_K) t_{\text{exch,Mg}} \frac{d\ln K_{\text{chd/g}}}{dt} (1 - \phi)^{-1} \text{(E.5)} \\ &= -0.13 f_{\text{evap,Mg}} \left(\frac{\overline{\text{Mg}}_{\text{max}}}{\text{Mg}_{\text{ARC}}} \right) \left(\frac{\alpha_{\text{Mg}}}{\alpha_K} \right) \frac{f_K (1 - f_K)}{0.2} t_{\text{exch,Mg}} \frac{d\ln K_{\text{chd/g}}}{dt} (1 - \phi)^{-1} \end{aligned}$$

with Mg_{ARC} the buffered concentration of Mg in the ARC, $\overline{\text{Mg}}_{\text{max}}$ the maximum average Mg concentration of the chondrules in the reservoir (that is, if Mg were all condensed) and $f_{\text{evap,Mg}}$ the evaporated fraction of Mg. The left-hand-side evaluates to -0.01, but may be brought in consistency with the right-hand-side by a low $f_{\text{evap,Mg}}$. Indeed, Mg is more refractory than K, and the low fraction of Mg in the gas phase allows preservation of (diluted) precursor isotopic signatures, while chondrule K has "forgotten" its beginnings.

References

Alexander, C.M.O., 1994. Trace element distributions within ordinary chondrite chondrules: Implications for chondrule formation conditions and precursors. *Geochimica et Cosmochimica Acta* 58, 3451–3467. doi:10.1016/0016-7037(94)90098-1.

Alexander, C.M.O., Grossman, J.N., 2005. Alkali elemental and potassium isotopic compositions of Semarkona chondrules. *Meteoritics and Planetary Science* 40, 541.

Alexander, C.M.O., Grossman, J.N., Ebel, D., 2007. Do We Need to Reassess the Formation Conditions of Chondrules?, in: 38th Annual Lunar and Planetary Science Conference, p. 2012.

Alexander, C.M.O., Grossman, J.N., Wang, J., Zanda, B., Bourot-Denise, M., Hewins, R.H., 2000. The lack of potassium-isotopic fractionation in Bishunpur chondrules. *Meteoritics and Planetary Science* 35, 859–868. doi:10.1111/j.1945-5100.2000.tb01469.x.

Alexander, C.M.O.D., Grossman, J.N., Ebel, D.S., Ciesla, F.J., 2008. The Formation Conditions of Chondrules and Chondrites. *Science* 320, 1617. doi:10.1126/science.1156561.

Arakawa, S., Nakamoto, T., 2019. Compound Chondrule Formation in Optically Thin Shock Waves. *The Astrophysical Journal* 877, 84. doi:10.3847/1538-4357/ab1b3e, [arXiv:1904.09580](https://arxiv.org/abs/1904.09580).

Asphaug, E., Jutzi, M., Movshovitz, N., 2011. Chondrule formation during planetesimal accretion. *Earth and Planetary Science Letters* 308, 369–379. doi:10.1016/j.epsl.2011.06.007.

Baecker, B., Rubin, A.E., Wasson, J.T., 2017. Secondary melting events in Semarkona chondrules revealed by compositional zoning in low-Ca pyroxene. *Geochimica et Cosmochimica Acta* 211, 256–279. doi:10.1016/j.gca.2017.05.013.

Barosch, J., Hezel, D.C., Ebel, D.S., Friend, P., 2019. Mineralogically zoned chondrules in ordinary chondrites as evidence for open system chondrule behaviour. *Geochimica et Cosmochimica Acta* 249, 1–16. doi:10.1016/j.gca.2019.01.018.

Berlin, J., 2009. Mineralogy and bulk chemistry of chondrules and matrix in petrologic type 3 chondrites. Ph.D. thesis. Freie Universitaet Berlin.

Boley, A.C., Morris, M.A., Desch, S.J., 2013. High-temperature Processing of Solids through Solar Nebular Bow Shocks: 3D Radiation Hydrodynamics Simulations with Particles. *The Astrophysical Journal* 776, 101. doi:10.1088/0004-637X/776/2/101, [arXiv:1308.2968](https://arxiv.org/abs/1308.2968).

Brearley, A.J., Jones, R.H., 1998. Chondritic meteorites, in: Papike, J.J. (Ed.), *Planetary Materials*. Mineralogical Society of America. chapter 3, pp. 3–1–3–398.

Chakraborty, S., 2010. Diffusion Coefficients in Olivine, Wadsleyite and Ringwoodite, in: Zhang, Y., Cherniak, D.J. (Eds.), *Diffusion in Minerals and Melts*. Mineralogical Society of America. volume 72 of *Reviews in Mineralogy & Geochemistry*, pp. 603–639.

Chaumard, N., Defouilloy, C., Kita, N.T., 2018. Oxygen isotope systematics of chondrules in the Murchison CM2 chondrite and implications for the CO-CM relationship. *Geochimica et Cosmochimica Acta* 228, 220–242. doi:10.1016/j.gca.2018.02.040.

Crank, J., 1975. The Mathematics of Diffusion. 2nd edition ed., Oxford University Press.

Cuzzi, J.N., Alexander, C.M.O., 2006. Chondrule formation in particle-rich nebular regions at least hundreds of kilometres across. *Nature* 441, 483–485. doi:10.1038/nature04834.

DeHart, J.M., 1989. Cathodoluminescence and microprobe studies of the unequilibrated ordinary chondrites. Ph.D. thesis. University of Arkansas, Little Rock.

Desch, S.J., Ciesla, F.J., Hood, L.L., Nakamoto, T., 2005. Heating of Chondritic Materials in Solar Nebula Shocks, in: A. N. Krot, E. R. D. Scott, & B. Reipurth (Ed.), *Chondrites and the Protoplanetary Disk*, pp. 849–871.

Desch, S.J., Cuzzi, J.N., 2000. The Generation of Lightning in the Solar Nebula. *Icarus* 143, 87–105. doi:10.1006/icar.1999.6245.

Desnoyers, C., 1980. The Niger (I) carbonaceous chondrite and implications for the origin of aggregates and isolated olivine grains in C2 chondrites. *Earth and Planetary Science Letters* 47, 223–234. doi:10.1016/0012-821X(80)90038-2.

Douglas-Song, T., Ota, T., Yamanaka, M., Kitagawa, H., Tanaka, R., Potiszil, C., Kunihiro, T., 2025. Lithium- and oxygen-isotope compositions of a Si-rich nebular reservoir determined from chondrule constituents in the Sahara 97103 EH3 chondrite. *Geochimica et Cosmochimica Acta* 400, 51–71. doi:10.1016/j.gca.2025.05.038.

Dullemond, C.P., Harsono, D., Stammler, S.M., Johansen, A., 2016. Forming Chondrules in Impact Splashes II Volatile Retention. *The Astrophysical Journal* 832, 91. doi:10.3847/0004-637X/832/1/91, arXiv:1608.03540.

Ebel, D.S., Grossman, L., 2000. Condensation in dust-enriched systems. *Geochimica et Cosmochimica Acta* 64, 339–366. doi:10.1016/S0016-7037(99)00284-7.

Fedkin, A.V., Grossman, L., 2013. Vapor saturation of sodium: Key to unlocking the origin of chondrules. *Geochimica et Cosmochimica Acta* 112, 226–250. doi:10.1016/j.gca.2013.02.020.

Fedkin, A.V., Grossman, L., Ghiorso, M.S., 2006. Vapor pressures and evaporation coefficients for melts of ferromagnesian chondrule-like compositions. *Geochimica et Cosmochimica Acta* 70, 206–223. doi:10.1016/j.gca.2005.08.014.

Florentin, L., Faure, F., Deloule, E., Tissandier, L., Gurenko, A., Lequin, D., 2017. Origin of Na in glass inclusions hosted in olivine from Allende CV3 and Jbilet Winselwan CM2: Implications for chondrule formation. *Earth and Planetary Science Letters* 474, 160–171. doi:10.1016/j.epsl.2017.06.038.

Friend, P., Hezel, D.C., Mucerschi, D., 2016. The conditions of chondrule formation, Part II: Open system. *Geochimica et Cosmochimica Acta* 173, 198–209. doi:10.1016/j.gca.2015.10.026.

Fuchs, L.H., Olsen, E., Jensen, K.J., 1973. Mineralogy and composition of the Murchison (C2) meteorite. *Smithsonian Contribution to the Earth Science* 10, 1–39.

Galy, A., Young, E.D., Ash, R.D., O’Nions, R.K., 2000. The Formation of Chondrules at High Gas Pressures in the Solar Nebula. *Science* 290, 1751–1754. doi:10.1126/science.290.5497.1751.

Georges, P., 2000. Volatilisation et condensation du potassium dans les silicates fondus: Approche expérimentale et thermodynamique, applications sidérurgiques et cosmochimiques. Ph.D. thesis. Université Henri Poincaré.

Gerber, S., Burkhardt, C., Budde, G., Metzler, K., Kleine, T., 2017. Mixing and Transport of Dust in the Early Solar Nebula as Inferred from Titanium Isotope Variations among Chondrules. *The Astrophysical Journal Letters* 841, L17. doi:10.3847/2041-8213/aa72a2, arXiv:1705.03676.

Ghiorso, M.S., Sack, R.O., 1995. Chemical mass transfer in magmatic processes IV. A revised and internally consistent thermodynamic model for the interpolation and extrapolation of liquid-solid equilibria in magmatic systems at elevated temperatures and pressures. *Contributions to Mineralogy and Petrology* 119, 197–212. doi:10.1007/BF00307281.

Gooding, J.L., Keil, K., 1981. Relative abundances of chondrule primary textural types in ordinary chondrites and their bearing on conditions of chondrule formation. *Meteoritics* 16, 17–43.

Grossman, J.N., Alexander, C.M.O., Ash, R.D., McDonough, W.F., 2007. Volatile Element Abundances in Chondrules Revisited: An LA-ICP-MS Study of QUE 97008 (LL3.05), in: 38th Annual Lunar and Planetary Science Conference, p. 2000.

Grossman, J.N., Alexander, C.M.O., Wang, J., Brearley, A.J., 2002. Zoned chondrules in Semarkona: Evidence for high- and low-temperature processing. *Meteoritics and Planetary Science* 37, 49–73. doi:10.1111/j.1945-5100.2002.tb00795.x.

Grossman, J.N., Rubin, A.E., Rambaldi, E.R., Rajan, R.S., Wasson, J.T., 1985. Chondrules in the Qingzhen type-3 enstatite chondrite Possible precursor components and comparison to ordinary chondrite chondrules. *Geochimica et Cosmochimica Acta* 49, 1781–1795. doi:10.1016/0016-7037(85)90149-8.

Grossman, L., Fedkin, A.V., Simon, S.B., 2012. Formation of the first oxidized iron in the solar system. *Meteoritics and Planetary Science* 47, 2160–2169. doi:10.1111/j.1945-5100.2012.01353.x.

Grossman, L., Simon, S.B., Rai, V.K., Thiemens, M.H., Hutcheon, I.D., Williams, R.W., Galy, A., Ding, T., Fedkin, A.V., Clayton, R.N., Mayeda, T.K., 2008. Primordial compositions of refractory inclusions. *Geochimica et Cosmochimica Acta* 72, 3001–3021.

Harju, E.R., Rubin, A.E., Ahn, I., Choi, B.G., Ziegler, K., Wasson, J.T., 2014. Progressive aqueous alteration of CR carbonaceous chondrites. *Geochimica et Cosmochimica Acta* 139, 267–292. doi:10.1016/j.gca.2014.04.048.

Hayashi, C., 1981. Structure of the Solar Nebula, Growth and Decay of Magnetic Fields and Effects of Magnetic and Turbulent Viscosities on the Nebula. *Progress of Theoretical Physics Supplement* 70, 35–53. doi:10.1143/PTPS.70.35.

Herbst, W., Greenwood, J.P., 2019. A radiative heating model for chondrule and chondrite formation. *Icarus* 329, 166–181. doi:10.1016/j.icarus.2019.03.039, arXiv:1903.12224.

Hewins, R.H., 1991. Retention of sodium during chondrule melting. *Geochimica et Cosmochimica Acta* 55, 935–942. doi:10.1016/0016-7037(91)90152-U.

Hewins, R.H., Radomsky, P.M., 1990. Temperature conditions for chondrule formation. *Meteoritics* 25, 309–318.

Hewins, R.H., Zanda, B., Bendersky, C., 2012. Evaporation and recondensation of sodium in Semarkona Type II chondrules. *Geochimica et Cosmochimica Acta* 78, 1–17. doi:10.1016/j.gca.2011.11.027.

Hezel, D.C., Kießwetter, R., 2010. Quantifying the error of 2D bulk chondrule analyses using a computer model to simulate chondrules (SIMCHON). *Meteoritics and Planetary Science* 45, 555–571. doi:10.1111/j.1945-5100.2010.01040.x.

Huang, S., Lu, J., Prinz, M., Weisberg, M.K., Benoit, P.H., Sears, D.W.G., 1996. Chondrules: Their Diversity and the Role of Open-System Processes during Their Formation. *Icarus* 122, 316–346. doi:10.1006/icar.1996.0127.

Humayun, M., 2012. Chondrule cooling rates inferred from diffusive profiles in metal lumps from the Acfer 097 CR2 chondrite. *Meteoritics and Planetary Science* , 169doi:10.1111/j.1945-5100.2012.01371.x.

Ichikawa, O., Ikeda, Y., 1995. Petrology of the Yamato-8449 CR chondrite. *Antarctic Meteorite Research* 8, 63.

Ikeda, Y., 1983. Major element chemical compositions and chemical types of chondrules in unequilibrated E, O, and C chondrites from Antarctica. *National Institute Polar Research Memoirs* 30, 122–145.

Ikeda, Y., 1989. Petrochemical study of the Yamato-691 enstatite chondrite (E3) V: Comparison of major element chemistries of chondrules and inclusions in Y-691 with those in ordinary and carbonaceous chondrites. *Antarctic Meteorite Research* 2, 147–165.

Ikeda, Y., Kimura, M., 1995. Anhydrous alteration of Allende chondrules in the solar nebula I: Description and alteration of chondrules with known oxygenisotopic compositions. *Antarctic Meteorite Research* 8, 97.

Ikeda, Y., Kimura, M., 1996. Anhydrous alteration of Allende chondrules in the solar nebula III: Alkali-zoned chondrules and heating experiments for anhydrous alteration. *Antarctic Meteorite Research* 9, 51.

Jacquet, E., 2014. The quasi-universality of chondrule size as a constraint for chondrule formation models. *Icarus* 232, 176–186.

Jacquet, E., 2021. Collisions and compositional variability in chondrule-forming events. *Geochimica et Cosmochimica Acta* 296, 18–37. doi:10.1016/j.gca.2020.12.025, arXiv:2101.10083.

Jacquet, E., 2022. Meteorite petrology versus genetics: Toward a unified binominal classification. *Meteoritics and Planetary Science* 57, 1774–1794. doi:10.1111/maps.13896, arXiv:2209.07377.

Jacquet, E., Alard, O., Gounelle, M., 2012. Chondrule trace element geochemistry at the mineral scale. *Meteoritics and Planetary Science* 47, 1695–1714. doi:10.1111/maps.12005.

Jacquet, E., Alard, O., Gounelle, M., 2015a. The formation conditions of enstatite chondrites: Insights from trace element geochemistry of olivine-bearing chondrules in Sahara 97096 (EH3). *Meteoritics and Planetary Science* 50, 1624–1642. doi:10.1111/maps.12481.

Jacquet, E., Alard, O., Gounelle, M., 2015b. Trace element geochemistry of ordinary chondrite chondrules: The type I/type II chondrule dichotomy. *Geochimica et Cosmochimica Acta* 155, 47–67. doi:10.1016/j.gca.2015.02.005.

Jacquet, E., Doisneau, B., 2024. The secondary classification of unequilibrated chondrites. *Meteoritics and Planetary Science* 59, 3150–3180. doi:10.1111/maps.14270, arXiv:2409.07838.

Jacquet, E., Dullemond, C., Drażkowska, J., Desch, S., 2024. The Early Solar System and Its Meteoritical Witnesses. *Space Science Reviews* 220, 78. doi:10.1007/s11214-024-01112-y, arXiv:2409.07212.

Jacquet, E., Marrocchi, Y., 2017. Chondrule heritage and thermal histories from trace element and oxygen isotope analyses of chondrules and amoeboid olivine aggregates. *Meteoritics and Planetary Science* 52, 2672–2694. doi:10.1111/maps.12985.

Johansen, A., Okuzumi, S., 2018. Harvesting the decay energy of ^{26}Al to drive lightning discharge in protoplanetary discs. *Astronomy and Astrophysics* 609, A31. doi:10.1051/0004-6361/201630047, arXiv:1708.05157.

Johnson, M.C., 1986. The solar nebula redox state as recorded by the most reduced chondrules of five primitive chondrites. *Geochimica et Cosmochimica Acta* 50, 1497–1502. doi:10.1016/0016-7037(86)90323-6.

Jones, R.H., 1990. Petrology and mineralogy of Type II, FeO-rich chondrules in Semarkona (LL3.0) - Origin by closed-system fractional crystallization, with evidence for supercooling. *Geochimica et Cosmochimica Acta* 54, 1785–1802. doi:10.1016/0016-7037(90)90408-D.

Jones, R.H., 1992. On the relationship between isolated and chondrule olivine grains in the carbonaceous chondrite ALHA77307. *Geochimica et Cosmochimica Acta* 56, 467–482. doi:10.1016/0016-7037(92)90145-9.

Jones, R.H., 1994. Petrology of FeO-poor, porphyritic pyroxene chondrules in the Semarkona chondrite. *Geochimica et Cosmochimica Acta* 58, 5325–5340. doi:10.1016/0016-7037(94)90316-6.

Jones, R.H., 1996. Relict grains in chondrules: evidence for chondrule recycling., in: R. H. Hewins, R. H. Jones, & E. R. D. Scott (Ed.), *Chondrules and the Protoplanetary Disk*, pp. 163–172.

Jones, R.H., Villeneuve, J., Libourel, G., 2018. Thermal Histories of Chondrules, in: Russell, S.S., Connolly, Harold C., J., Krot, A.N. (Eds.), *Chondrules: Records of Protoplanetary Disk Processes*, pp. 57–90. doi:10.1017/9781108284073.003.

Kimura, M., Ikeda, Y., 1995. Anhydrous alteration of Allende chondrules in the solar nebula II: Alkali-Ca exchange reactions and formation of nepheline, sodalite and Ca-rich phases in chondrules. *Antarctic Meteorite Research* 8, 123.

Kimura, M., Ikeda, Y., 1997. Comparative study of anhydrous alteration of chondrules in reduced and oxidized CV chondrites. *Antarctic Meteorite Research* 10, 191.

Kimura, M., Ikeda, Y., 1998. Hydrous and anhydrous alterations of chondrules in Kaba and Mokoia CV chondrites. *Meteoritics and Planetary Science* 33, 1139–1146. doi:10.1111/j.1945-5100.1998.tb01718.x.

Kimura, M., Imae, N., Komatsu, M., Barrat, J.A., Greenwood, R.C., Yamaguchi, A., Noguchi, T., 2020. The most primitive CM chondrites, Asuka 12085, 12169, and 12236, of subtypes 3.0-2.8: Their characteristic features and classification. *Polar Science* 26, 100565. doi:10.1016/j.polar.2020.100565.

Kita, N.T., Nagahara, H., Tachibana, S., Tomomura, S., Spicuzza, M.J., Fournelle, J.H., Valley, J.W., 2010. High precision SIMS oxygen three isotope study of chondrules in LL3 chondrites: Role of ambient gas during chondrule formation. *Geochimica et Cosmochimica Acta* 74, 6610–6635. doi:10.1016/j.gca.2010.08.011.

Koefoed, P., Barrat, J.A., Pravdivtseva, O., Alexander, C.M.O., Lodders, K., Ogliore, R., Wang, K., 2023. The potassium isotopic composition of CI chondrites and the origin of isotopic variations among primitive planetary bodies. *Geochimica et Cosmochimica Acta* 358, 49–60. doi:10.1016/j.gca.2023.07.025.

Koefoed, P., Wang, K., 2025. Unravelling chondrule formation processes: Clues from the potassium isotopic composition of chondrules from un-equilibrated ordinary chondrites. *Geochimica et Cosmochimica Acta* 398, 163–177. doi:10.1016/j.gca.2025.04.012.

Kracher, A., Keil, K., Kallemeyn, G.W., Wasson, J.T., Clayton, R.N., Huss, G.I., 1985. The Leoville (CV3) accretionary breccia. *Lunar and Planetary Science Conference Proceedings* 90, D123–D135.

Krot, A.N., Ivanova, M.A., Ulyanov, A.A., 2007. Chondrules in the CB/CH-like carbonaceous chondrite Isheyevo: Evidence for various chondrule-forming mechanisms and multiple chondrule generations. *Chemie der Erde - Geochemistry* 67, 283 – 300. URL: <http://www.sciencedirect.com/science/article/B7CW6-4M04J9X-1/2/3a2fd5643815d5ec2> doi:DOI: 10.1016/j.chemer.2006.04.001.

Krot, A.N., McKeegan, K.D., Huss, G.R., Liffman, K., Sahijpal, S., Hutcheon, I.D., Srinivasan, G., Bischoff, A., Keil, K., 2006. Aluminum-

Magnesium and Oxygen Isotope Study of Relict Ca-Al-rich Inclusions in Chondrules. The Astrophysical Journal 639, 1227–1237. doi:10.1086/498610.

Krot, A.N., Nagashima, K., Ciesla, F.J., Meyer, B.S., Hutcheon, I.D., Davis, A.M., Huss, G.R., Scott, E.R.D., 2010. Oxygen Isotopic Composition of the Sun and Mean Oxygen Isotopic Composition of the Protosolar Silicate Dust: Evidence from Refractory Inclusions. The Astrophysical Journal 713, 1159–1166. doi:10.1088/0004-637X/713/2/1159.

Krot, A.N., Petaev, M.I., Russell, S.S., Itoh, S., Fagan, T.J., Yurimoto, H., Chizmadia, L., Weisberg, M.K., Komatsu, M., Ulyanov, A.A., Keil, K., 2004. Amoeboid olivine aggregates and related objects in carbonaceous chondrites: records of nebular and asteroid processes. *Chemie der Erde / Geochemistry* 64, 185–239. doi:10.1016/j.chemer.2004.05.001.

Krot, A.N., Petaev, M.I., Scott, E.R.D., Choi, B.G., Zolensky, M.E., Keil, K., 1998. Progressive alteration in CV3 chondrites: More evidence for asteroidal alteration. *Meteoritics and Planetary Science* 33, 1065–1085. doi:10.1111/j.1945-5100.1998.tb01713.x.

Lauretta, D.S., Connolly, H.C., Aebersold, J.E., Alexander, C.M.O., Ballouz, R.L., Barnes, J.J., Bates, H.C., Bennett, C.A., Blanche, L., Blumenfeld, E.H., Clemett, S.J., Cody, G.D., DellaGiustina, D.N., Dworkin, J.P., Eckley, S.A., Foustaoukos, D.I., Franchi, I.A., Glavin, D.P., Greenwood, R.C., Haenecour, P., Hamilton, V.E., Hill, D.H., Hiroi, T., Ishimaru, K., Jourdan, F., Kaplan, H.H., Keller, L.P., King, A.J., Koefoed, P., Kontogiannis, M.K., Le, L., Macke, R.J., McCoy, T.J., Milliken, R.E., Najorka, J., Nguyen, A.N., Pajola, M., Polit, A.T., Righter, K., Roper, H.L., Russell, S.S., Ryan, A.J., Sandford, S.A., Schofield, P.F., Schultz, C.D., Seifert, L.B., Tachibana, S., Thomas-Keprta, K.L., Thompson, M.S., Tu, V., Tusberti, F., Wang, K., Zega, T.J., Wolner, C.W.V., 2024. Asteroid (101955) Bennu in the laboratory: Properties of the sample collected by OSIRIS-REx. *Meteoritics and Planetary Science* 59, 2453–2486. doi:10.1111/maps.14227, arXiv:2404.12536.

Lesher, C.E., 2010. Self-diffusion in Silicate Melts: Theory, Observations and Applications to Magmatic Systems, in: Zhang, Y., Cherniak, D.J. (Eds.), *Diffusion in Minerals and Melts*. Mineralogical Society of America. volume 72 of *Reviews in Mineralogy & Geochemistry*, pp. 269–309.

Libourel, G., Krot, A.N., Tissandier, L., 2003. Evidence for High Temperature Condensation of Moderately-Volatile Elements During Chondrule Formation, in: Mackwell, S., Stansbery, E. (Eds.), Lunar and Planetary Institute Science Conference Abstracts, p. 1558.

Libourel, G., Krot, A.N., Tissandier, L., 2006. Role of gas-melt interaction during chondrule formation. *Earth and Planetary Science Letters* 251, 232–240. doi:10.1016/j.epsl.2006.09.011.

Libourel, G., Nagashima, K., Portail, M., Krot, A.N., 2023. On the significance of oxygen-isotope variations in chondrules from carbonaceous chondrites. *Geochimica et Cosmochimica Acta* 346, 102–120. doi:10.1016/j.gca.2023.01.026.

Libourel, G., Portail, M., 2018. Chondrules as direct thermochemical sensors of solar protoplanetary disk gas. *Science Advances* 4, eaar3321.

Lodders, K., 2003. Solar System Abundances and Condensation Temperatures of the Elements. *The Astrophysical Journal* 591, 1220–1247. doi:10.1086/375492.

Lodders, K., Fegley, B., Mezger, K., Ebel, D., 2025. Condensation and the Volatility Trend of the Earth. *Space Science Reviews* 221, 54. doi:10.1007/s11214-025-01182-6, arXiv:2411.01362.

Lowry, R.K., Henderson, P., Nolan, J., 1982. Tracer diffusion of some alkali, alkaline-earth and transition element ions in a basaltic and an andesitic melt and the implications concerning melt structure. *Contributions to Mineralogy and Petrography* 80, 254–261.

Mahlé, T., Marrocchi, Y., Neukampf, J., Villeneuve, J., Jacquet, E., 2024. The last generation of nebular chondrules possibly sampled in the CH/CB_b chondrite Isheyev. *Geochimica et Cosmochimica Acta* 385, 74–86. doi:10.1016/j.gca.2024.08.027.

Marrocchi, Y., Euverte, R., Villeneuve, J., Batanova, V., Welsch, B., Ferrière, L., Jacquet, E., 2019. Formation of CV chondrules by recycling of amoeboid olivine aggregate-like precursors. *Geochimica et Cosmochimica Acta* 247, 121–141. doi:10.1016/j.gca.2018.12.038.

Marrocchi, Y., Jones, R.H., Russell, S.S., Hezel, D.C., Barosch, J., Kuznetsova, A., 2024. Chondrule Properties and Formation Conditions. *Space Science Reviews* 220, 69. doi:10.1007/s11214-024-01102-0.

Marrocchi, Y., Villeneuve, J., Batanova, V., Piani, L., Jacquet, E., 2018. Oxygen isotopic diversity of chondrule precursors and the nebular origin of chondrules. *Earth and Planetary Science Letters* 496, 132–141. doi:10.1016/j.epsl.2018.05.042.

Mathieu, R., 2009. Solubilité du sodium dans les silicates fondus. Ph.D. thesis. Institut National Polytechnique de Lorraine.

Mathieu, R., Libourel, G., Deloule, E., Tissandier, L., Rapin, C., Podor, R., 2011. Na₂O solubility in CaO-MgO-SiO₂ melts. *Geochimica et Cosmochimica Acta* 75, 608–628. doi:10.1016/j.gca.2010.11.001.

Matsuda, H., Nakamura, N., Noda, S., 1990. Alkali (Rb/K) Abundances in Allende Barred-Olivine Chondrules: Implications for the Melting Conditions of Chondrules. *Meteoritics* 25, 137. doi:10.1111/j.1945-5100.1990.tb00985.x.

Matsunami, S., Ninagawa, K., Nishimura, S., Kubono, N., Yamamoto, I., Kohata, M., Wada, T., Yamashita, Y., Lu, J., Sears, D.W.G., Nishimura, H., 1993. Thermoluminescence and compositional zoning in the mesostasis of a Semarkona group A1 chondrule and new insights into the chondrule-forming process. *Geochimica et Cosmochimica Acta* 57, 2101–2110. doi:10.1016/0016-7037(93)90096-F.

Misawa, K., Nakamura, N., 1988. Demonstration of REE fractionation among individual chondrules from the Allende (CV3) chondrite. *Geochimica et Cosmochimica Acta* 52, 1699–1710. doi:10.1016/0016-7037(88)90238-4.

Miyamoto, M., Mikouchi, T., Jones, R.H., 2009. Cooling rates of porphyritic olivine chondrules in the Semarkona (LL3.00) ordinary chondrite: A model for diffusional equilibration of olivine during fractional crystallization. *Meteoritics and Planetary Science* 44, 521–530. doi:10.1111/j.1945-5100.2009.tb00748.x.

Mokhtari, M., Bourdon, B., 2026. Condensation of major and trace elements in dust-rich environments. *Icarus* 444, 116801. URL:

<https://www.sciencedirect.com/science/article/pii/S0019103525003495>,
doi:<https://doi.org/10.1016/j.icarus.2025.116801>.

Morin, G.L.F., Marrocchi, Y., Villeneuve, J., Jacquet, E., 2022. ^{16}O -rich anhydrous silicates in CI chondrites: Implications for the nature and dynamics of dust in the solar accretion disk. *Geochimica et Cosmochimica Acta* 332, 203–219. doi:[10.1016/j.gca.2022.06.017](https://doi.org/10.1016/j.gca.2022.06.017).

Morton, E.M., Pickard, H., Wombacher, F., Huang, Y., Palk, E., Martins, R., Kuthning, S., Schönbächler, M., Rehkämper, M., 2024. Volatile Element Depletion of Carbonaceous Chondrites—Insights from Mass-dependent Zinc, Cadmium, and Tellurium Isotope Variations. *The Astrophysical Journal* 977, 53. doi:[10.3847/1538-4357/ad87ed](https://doi.org/10.3847/1538-4357/ad87ed).

Mungall, J.E., 2002. Empirical models relating viscosity and tracer diffusion in magmatic silicate melts. *Geochimica et Cosmochimica Acta* 66, 125–143. doi:[10.1016/S0016-7037\(01\)00736-0](https://doi.org/10.1016/S0016-7037(01)00736-0).

Nagahara, H., Kita, N.T., Ozawa, K., Morishita, Y., 2008. Condensation of major elements during chondrule formation and its implication to the origin of chondrules. *Geochimica et Cosmochimica Acta* 72, 1442–1465. doi:[10.1016/j.gca.2007.12.020](https://doi.org/10.1016/j.gca.2007.12.020).

Nakamura, T., Matsumoto, M., Amano, K., Enokido, Y., Zolensky, M.E., Mikouchi, T., Genda, H., Tanaka, S., Zolotov, M.Y., Kurosawa, K., Wakita, S., Hyodo, R., Nagano, H., Nakashima, D., Takahashi, Y., Fujioka, Y., Kikuri, M., Kagawa, E., Matsuoka, M., Brearley, A.J., Tsuchiyama, A., Uesugi, M., Matsuno, J., Kimura, Y., Sato, M., Milliken, R.E., Tatsumi, E., Sugita, S., Hiroi, T., Kitazato, K., Brownlee, D., Joswiak, D.J., Takahashi, M., Ninomiya, K., Takahashi, T., Osawa, T., Terada, K., Brenker, F.E., Tkalcic, B.J., Vincze, L., Brunetto, R., Aléon-Toppani, A., Chan, Q.H.S., Roskosz, M., Viennet, J.C., Beck, P., Alp, E.E., Michikami, T., Nagaashi, Y., Tsuji, T., Ino, Y., Martinez, J., Han, J., Dolocan, A., Bodnar, R.J., Tanaka, M., Yoshida, H., Sugiyama, K., King, A.J., Fukushi, K., Suga, H., Yamashita, S., Kawai, T., Inoue, K., Nakato, A., Noguchi, T., Vilas, F., Hendrix, A.R., Jaramillo-Correa, C., Domingue, D.L., Dominguez, G., Gainsforth, Z., Engrand, C., Duprat, J., Russell, S.S., Bonato, E., Ma, C., Kawamoto, T., Wada, T., Watanabe, S., Endo, R., Enju, S., Riu, L., Rubino, S., Tack, P., Takeshita, S., Takeichi, Y., Takeuchi, A., Takir, D., Tanigaki, T., Taniguchi,

A., Tsukamoto, K., Yagi, T., Yamada, S., Yamamoto, K., Yamashita, Y., Yasutake, M., Uesugi, K., Umegaki, I., Chiu, I., Ishizaki, T., Okumura, S., Palomba, E., Pilarget, C., Potin, S.M., Alasli, A., Anada, S., Araki, Y., Sakatani, N., Schultz, C., Sekizawa, O., Sitzman, S.D., Sugiura, K., Sun, M., Dartois, E., De Pauw, E., Dionnet, Z., Djouadi, Z., Falkenberg, G., Fujita, R., Fukuma, T., Gearba, I.R., Hagiya, K., Hu, M.Y., Kato, T., Kawamura, T., Kimura, M., Kubo, M.K., Langenhorst, F., Lantz, C., Lavina, B., Lindner, M., Zhao, J., Vekemans, B., Baklouti, D., Bazi, B., Borondics, F., Nagasawa, S., Nishiyama, G., Nitta, K., Mathurin, J., Matsumoto, T., Mitsukawa, I., Miura, H., Miyake, A., Miyake, Y., Yurimoto, H., Okazaki, R., Yabuta, H., Naraoka, H., Sakamoto, K., Tachibana, S., Connolly, H.C., Lauretta, D.S., Yoshitake, M., Yoshikawa, M., Yoshikawa, K., Yoshihara, K., Yokota, Y., Yogata, K., Yano, H., Yamamoto, Y., Yamamoto, D., Yamada, M., Yamada, T., Yada, T., Wada, K., Usui, T., Tsukizaki, R., Terui, F., Takeuchi, H., Takei, Y., Iwamae, A., Soejima, H., Shirai, K., Shimaki, Y., Senshu, H., Sawada, H., Saiki, T., Ozaki, M., Ono, G., Okada, T., Ogawa, N., Ogawa, K., Noguchi, R., Noda, H., Nishimura, M., Namiki, N., Nakazawa, S., Morota, T., Miyazaki, A., Miura, A., Mimasu, Y., Matsumoto, K., Kumagai, K., Kouyama, T., Kikuchi, S., Kawahara, K., Kameda, S., Iwata, T., Ishihara, Y., Ishiguro, M., Ikeda, H., Hosoda, S., Honda, R., Honda, C., Hitomi, Y., Hirata, N., Hirata, N., Hayashi, T., Hayakawa, M., Hatakeyama, K., Furuya, S., Fukai, R., Fujii, A., Cho, Y., Arakawa, M., Abe, M., Watanabe, S., Tsuda, Y., 2023. Formation and evolution of carbonaceous asteroid Ryugu: Direct evidence from returned samples. *Science* 379, abn8671. doi:10.1126/science.abn8671.

Nakashima, D., Noguchi, T., Ushikubo, T., Kimura, M., Kita, N., 2024. Oxygen isotope study of the Asuka-881020 CH chondrite II: Porphyritic chondrules. *Geochimica et Cosmochimica Acta* 373, 292–307. doi:10.1016/j.gca.2024.04.011.

Nie, N.X., Chen, X.Y., Hopp, T., Hu, J.Y., Zhang, Z.J., Teng, F.Z., Shahar, A., Dauphas, N., 2021. Imprint of chondrule formation on the K and Rb isotopic compositions of carbonaceous meteorites. *Science Advances* 7, eabl3929. doi:10.1126/sciadv.abl3929.

Nie, N.X., Wang, D., Torrano, Z.A., Carlson, R.W., O'D. Alexander, C.M., Shahar, A., 2023. Meteorites have inherited nucleosynthetic anomalies.

lies of potassium-40 produced in supernovae. *Science* 379, 372–376. doi:10.1126/science.abn1783.

Olsen, E.J., 1983. SiO₂-bearing Chondrules in the Murchison (C2) meteorite, in: King, E.A. (Ed.), *Chondrules and their Origins*, pp. 223–234.

Ozawa, K., Nagahara, H., 2001. Chemical and isotopic fractionations by evaporation and their cosmochemical implications. *Geochimica et Cosmochimica Acta* 65, 2171–2199. doi:10.1016/S0016-7037(01)00578-6.

Piani, L., Marrocchi, Y., Libourel, G., Tissandier, L., 2016. Magmatic sulfides in the porphyritic chondrules of EH enstatite chondrites. *Geochimica et Cosmochimica Acta* 195, 84–99. doi:10.1016/j.gca.2016.09.010, arXiv:1609.08750.

Pinto, G.A., Jacquet, E., Corgne, A., Olivares, F., Villeneuve, J., Marrocchi, Y., 2024. Deciphering recycling processes during solar system evolution from magnesium-rich relict olivine grains in type II chondrules. *Geochimica et Cosmochimica Acta* 364, 65–78. doi:10.1016/j.gca.2023.11.012.

Piralla, M., Villeneuve, J., Batanova, V., Jacquet, E., Marrocchi, Y., 2021. Conditions of chondrule formation in ordinary chondrites. *Geochimica et Cosmochimica Acta* 313, 295–312. doi:10.1016/j.gca.2021.08.007.

Richter, F.M., 2004. Timescales determining the degree of kinetic isotope fractionation by evaporation and condensation. *Geochimica et Cosmochimica Acta* 68, 4971–4992. doi:10.1016/j.gca.2004.06.008.

Richter, F.M., Mendybaev, R.A., Christensen, J., Gaffney, A., Ebel, D., 2009. Elemental and Isotope Fractionation of Chondrule-like Liquids by Evaporation into Vacuum, in: *Lunar and Planetary Institute Science Conference Abstracts*, p. 2321.

Rubin, A.E., 2024. Differences in bulk Fe content and density between type I and type II ordinary chondrite chondrules: Implications for parent body heterogeneities in oxidation state and O-isotopic composition. *Meteoritics and Planetary Science* 59, 2403–2410. doi:10.1111/maps.14223.

Rubin, A.E., Wasson, J.T., 1988. Chondrules and matrix in the Ornans CO3 meteorite: Possible precursor components. *Geochimica et Cosmochimica Acta* 52, 425–432. doi:10.1016/0016-7037(88)90098-1.

Rubin, A.E., Wasson, J.T., 2005. Non-spherical lobate chondrules in CO3.0 Y-81020: General implications for the formation of low-FeO porphyritic chondrules in CO chondrites. *Geochimica et Cosmochimica Acta* 69, 211–220. doi:10.1016/j.gca.2004.06.019.

Ruzicka, A., 2012. Chondrule formation by repeated evaporative melting and condensation in collisional debris clouds around planetesimals. *Meteoritics and Planetary Science* 47, 2218–2236. doi:10.1111/j.1945-5100.2012.01412.x.

Ruzicka, A., Floss, C., Hutson, M., 2012. Agglomeratic olivine (AO) objects and Type II chondrules in ordinary chondrites: Accretion and melting of dust to form ferroan chondrules. *Geochimica et Cosmochimica Acta* 76, 103–124. doi:10.1016/j.gca.2011.10.020.

Sanders, I.S., Scott, E.R.D., 2012. The origin of chondrules and chondrites: Debris from low-velocity impacts between molten planetesimals? *Meteoritics and Planetary Science* 47, 2170–2192. doi:10.1111/maps.12002.

Savage, P.S., Moynier, F., Boyet, M., 2022. Zinc isotope anomalies in primitive meteorites identify the outer solar system as an important source of Earth’s volatile inventory. *Icarus* 386, 115172. doi:10.1016/j.icarus.2022.115172.

Schneider, D.M., Symes, S.J.K., Benoit, P.H., Sears, D.W.G., 2002. Properties of chondrules in EL3 chondrites, comparison with EH3 chondrites, and the implications for the formation of enstatite chondrites. *Meteoritics and Planetary Science* 37, 1401–1416. doi:10.1111/j.1945-5100.2002.tb01037.x.

Schneider, J.M., Burkhardt, C., Marrocchi, Y., Brennecke, G.A., Kleine, T., 2020. Early evolution of the solar accretion disk inferred from Cr-Ti-O isotopes in individual chondrules. *Earth and Planetary Science Letters* 551, 116585. doi:10.1016/j.epsl.2020.116585, arXiv:2009.08684.

Seitz, H.M., Brey, G.P., Zipfel, J., Ott, U., Weyer, S., Durali, S., Weinbruch, S., 2007. Lithium isotope composition of ordinary and carbonaceous chondrites, and differentiated planetary bodies: Bulk solar system and solar reservoirs. *Earth and Planetary Science Letters* 260, 582–596. doi:10.1016/j.epsl.2007.06.019.

Seitz, H.M., Zipfel, J., Brey, G.P., Ott, U., 2012. Lithium isotope compositions of chondrules, CAI and a dark inclusion from Allende and ordinary chondrites. *Earth and Planetary Science Letters* 329, 51–59. doi:10.1016/j.epsl.2012.02.015.

Sekiya, M., Nakamura, T., 1996. Condition for the formation of the compound chondrules in the solar nebula. *Antarctic Meteorite Research* 9, 208.

Smith, A., Jones, R.H., 2024. Petrographic constraints on the formation of silica-rich igneous rims around chondrules in CR chondrites. *Meteoritics and Planetary Science* 59, 685–718. doi:10.1111/maps.14051.

Sossi, P.A., Hin, R.C., Kleine, T., Morbidelli, A., Nimmo, F., 2025. Physicochemical Controls on the Compositions of the Earth and Planets. *Space Science Reviews* 221, 118. doi:10.1007/s11214-025-01243-w, arXiv:2512.00373.

Sossi, P.A., Klemme, S., O'Neill, H.S.C., Berndt, J., Moynier, F., 2019. Evaporation of moderately volatile elements from silicate melts: experiments and theory. *Geochimica et Cosmochimica Acta* 260, 204–231. doi:10.1016/j.gca.2019.06.021.

Soulié, C., 2014. Formation des chondres et relation avec leurs auréoles de matrice à grains fins. Ph.D. thesis. Université de Lorraine.

Soulié, C., Libourel, G., Tissandier, L., 2017. Olivine dissolution in molten silicates: An experimental study with application to chondrule formation. *Meteoritics and Planetary Science* 52, 225–250.

Spandler, C., O'Neill, H.S.C., 2009. Diffusion and partition coefficients of minor and trace elements in San Carlos olivine at 1,300 C with some geochemical implications. *Contributions to Mineralogy and Petrology* 159, 791–818.

Stull, D.R., Prophet, H., 1971. Janaf thermochemical tables, second edition:. doi:<https://doi.org/10.6028/NBS.NSRDS.37>.

Tachibana, S., Nagahara, H., Mostefaoui, S., Kita, N.T., 2003. Correlation between relative ages inferred from ^{26}Al and bulk compositions of ferromagnesian chondrules in least equilibrated ordinary chondrites. *Meteoritics and Planetary Science* 38, 939–962.

Tenner, T.J., Nakashima, D., Ushikubo, T., Kita, N.T., Weisberg, M.K., 2015. Oxygen isotope ratios of FeO-poor chondrules in CR3 chondrites: Influence of dust enrichment and H₂O during chondrule formation. *Geochimica et Cosmochimica Acta* 148, 228–250. doi:10.1016/j.gca.2014.09.025.

Tenner, T.J., Ushikubo, T., Kurahashi, E., Kita, N.T., Nagahara, H., 2013. Oxygen isotope systematics of chondrule phenocrysts from the CO3.0 chondrite Yamato 81020: Evidence for two distinct oxygen isotope reservoirs. *Geochimica et Cosmochimica Acta* 102, 226–245. doi:10.1016/j.gca.2012.10.034.

Tissandier, L., Libourel, G., Robert, F., 2002. Gas-melt interactions and their bearing on chondrule formation. *Meteoritics and Planetary Science* 37, 1377–1389. doi:10.1111/j.1945-5100.2002.tb01035.x.

Tsuchiyama, A., Nagahara, H., Kushiro, I., 1981. Volatilization of sodium from silicate melt spheres and its application to the formation of chondrules. *Geochimica et Cosmochimica Acta* 45, 1357–1367. doi:10.1016/0016-7037(81)90228-3.

Ushikubo, T., Kimura, M., Kita, N.T., Valley, J.W., 2012. Primordial oxygen isotope reservoirs of the solar nebula recorded in chondrules in Acfer 094 carbonaceous chondrite. *Geochimica et Cosmochimica Acta* 90, 242–264. doi:10.1016/j.gca.2012.05.010.

Varela, M.E., Kurat, G., 2009. Glasses in meteorites and the primary liquid condensation model. *Mitteilungen der Österreichischen Mineralogischen Gesellschaft* 155, 279–320.

Varela, M.E., Kurat, G., Hoppe, P., Brandstätter, F., 2002. Chemistry of glass inclusions in olivines of the CR chondrites Renazzo, Acfer 182, and El Djouf 001. *Geochimica et Cosmochimica Acta* 66, 1663–1679. doi:10.1016/S0016-7037(01)00871-7.

Varela, M.E., Kurat, G., Zinner, E., 2005. A liquid-supported condensation of major minerals in the solar nebula: Evidence from glasses in the Kaba (CV3) chondrite. *Icarus* 178, 553–569. doi:10.1016/j.icarus.2005.05.001.

Villeneuve, J., 2010. Formation des chondres : précurseurs et chronologie. Ph.D. thesis. Ecole Doctorale Sciences et Ingénieurs des Ressources, Procédés, Produits, Environnements.

Villeneuve, J., Libourel, G., Soulié, C., 2015. Relationships between type I and type II chondrules: Implications on chondrule formation processes. *Geochimica et Cosmochimica Acta* 160, 277–305. doi:10.1016/j.gca.2015.03.033.

Wang, B., Moynier, F., Hu, Y., 2025. Rubidium and potassium isotope compositions of enstatite meteorites: implications for the evolution of their parent body(ies). *Geochimica et Cosmochimica Acta* 397, 63–74. doi:10.1016/j.gca.2025.04.007.

Wasson, J.T., Rubin, A.E., 2010. Metal in CR chondrites. *Geochimica et Cosmochimica Acta* 74, 2212–2230. doi:10.1016/j.gca.2010.01.014.

Weinbruch, S., Müller, W.F., Hewins, R.H., 2001. A transmission electron microscope study of exsolution and coarsening in iron-bearing clinopyroxene from synthetic analogues of chondrules. *Meteoritics and Planetary Science* 36, 1237–1248. doi:10.1111/j.1945-5100.2001.tb01957.x.

Wick, M.J., Jones, R.H., 2012. Formation conditions of plagioclase-bearing type I chondrules in CO chondrites: A study of natural samples and experimental analogs. *Geochimica et Cosmochimica Acta* 98, 140–159. doi:10.1016/j.gca.2012.09.027.

Wolf, A.S., Jäggi, N., Sossi, P.A., Bower, D.J., 2023. VapoRock: Thermodynamics of Vaporized Silicate Melts for Modeling Volcanic Outgassing and Magma Ocean Atmospheres. *The Astrophysical Journal* 947, 64. doi:10.3847/1538-4357/acbcc7, arXiv:2208.09582.

Wölfer, E., Burkhardt, C., Nimmo, F., Kleine, T., 2025. Origin of moderately volatile elements in Earth inferred from mass-dependent Ge isotope variations among chondrites. *Earth and Planetary Science Letters* 663, 119435. doi:10.1016/j.epsl.2025.119435, arXiv:2505.06604.

Wood, J.A., 1967. Chondrites: Their metallic minerals, thermal histories, and parent planets. *Icarus* 6, 1–49. doi:10.1016/0019-1035(67)90002-4.

Yu, Y., Hewins, R.H., Alexander, C.M.O.D., Wang, J., 2003. Experimental study of evaporation and isotopic mass fractionation of potassium in silicate melts. *Geochimica et Cosmochimica Acta* 67, 773–786. doi:10.1016/S0016-7037(02)01176-6.

Zhang, A.C., Hsu, W.B., Floss, C., Li, X.H., Li, Q.L., Liu, Y., Taylor, L.A., 2010. Petrogenesis of lunar meteorite Northwest Africa 2977: Constraints from in situ microprobe results. *Meteoritics and Planetary Science* 45, 1929–1947. doi:10.1111/j.1945-5100.2010.01131.x.

Zhang, M., Lin, Y., Tang, G., Liu, Y., Leya, I., 2020. Origin of Al-rich chondrules in CV chondrites: Incorporation of diverse refractory components into the ferromagnesian chondrule-forming region. *Geochimica et Cosmochimica Acta* 272, 198–217. doi:10.1016/j.gca.2019.12.011.

Zhang, Z.J., Nie, N.X., Mandybaev, R.A., Liu, M.C., Hu, J.J., Hopp, T., Alp, E.E., Lavina, B., Bullock, E.S., McKeegan, K.D., Dauphas, N., 2021. Loss and Isotopic Fractionation of Alkali Elements during Diffusion-Limited Evaporation from Molten Silicate: Theory and Experiments. *ACS Earth and Space Chemistry* 5, 755–784. doi:10.1021/acsearthspacechem.0c00263.